공학박사학위논문

Directed Self-Assembly of Polyelectrolytes & Charged Block Copolymer Micelles in Aqueous Media

수용액상의 고분자전해질 및 전하를 띤 블록공중합체 미셀의 유도조립에 관한 연구

2013년 8월

서울대학교대학원

화학생물공학부

이미숙

Abstract

Directed Self-Assembly of Polyelectrolytes & Charged Block Copolymer Micelles in Aqueous Media

Misook Lee
School of Chemical and Biological Engineering
The Graduate School
Seoul National University

Polyelectrolyte complexes (PECs) have received a growing interest since the early sixties. PECs have been used for large-scale industrial applications and have demonstrated enormous potentials in various fields such as coatings, binders and flocculants. Using the Layer-by-layer (LbL) deposition technique, an ultrathin polyelectrolyte multilayer (PEMs) coating was first built in 1990 and soon both theoretical and practical interest in these coatings were growing exponentially.

In the first chapter of this dissertation, we demonstrate that polyelectrolyte (PE) multilayer thin films deposited on patterned posts with incredibly large numbers of bilayers, which would not be possible with the conventional LbL deposition methods, can be obtained in short process time using alternating polyelectrolyte droplets generated in a microfluidic channel, representing a significant advantage over the conventional processes based on the polyelectrolyte deposition followed by the separation of such substrates (typically colloidal particles) with centrifugation and sonication. Positively- and negatively-charged

polyelectrolyte droplets were alternatively generated in a microfluidic channel by controlling the capillary number (Ca) as well as the fraction of dispersed phase over the continuous phase. Patterned posts, serving as the substrates for the PE deposition, were created with photo-curable polymers using the optofluidic maskless lithography. The impact of these PE droplets onto the patterned posts allowed the alternative adsorption of PEs, similar to the conventional LbL deposition methods. It was shown that the intensity of fluorescence dye tagged onto (+)-charged PEs adsorbed on the post(s), taken with confocal laser scanning microscopy, increases with deposition time and varies around the post(s). The effect of post shape and interval between the two posts for the droplet-based LbL deposition was also experimentally investigated and analyzed, in connection with the numerical simulations, to elucidate the underlying principles of relevant two-phase flows.

In the second chapter, we demonstrated block copolymer micelle (BCM) / BCM multilayer films with a large number of bilayers onto microposts using alternating droplets in cross-shaped microfluidic channels. Alternating aqueous droplets containing oppositely charged BCMs were employed for sequential adsorption onto microposts in a specific range of capillary numbers (Ca), resulting in the production of BCM multilayer films with thicknesses of hundreds of nanometers requiring a small amount of the BCM solution in a short process time. To date, it has not been possible to deposit a large amount of BCMs onto colloidal substrates without a multi-step process involving steps such as centrifugation and redispersion by sonication to proceed to next deposition step. In addition, cross-shaped microfluidic channels with BCMs deposited onto posts were utilized for the visualization of selective and continuous destruction of the BCM multilayer films using two different laminar streams, basic distilled water as a release solvent and oleic acid as a non-reactive medium, since the ionization of cationic segments is negligible above a pH of 5.5. As a result, the

BCM multilayer films were selectively removed from the posts by contact with the aqueous release solvent. In the case of BCMs touched with the non-reactive medium, the decrease of the fluorescence intensity on the BCMs, which is only modulated by the shear rate, was negligible at the same processing time.

In the third chapter, we demonstrated the complexes of oppositely charged polystyrene-block-poly(acrylic acid) (PS-b-PAA) micelles and polystyrene-block-poly(4-vinyl pyridine) (PS-b-P4VP) micelles. In generally, complexation of soft colloids can induce novel morphologies unlike packing problem of hard particles since deformable interface of soft colloids can be easily tuned by inter-corona repulsion or packing parameters. In the present study, complex morphology of charged BCMs was controlled by pH of aqueous solvent as well as solvent quality. To determine the effective pH range for the inter-corona combination of PAA and P4VP blocks in aqueous media, we studied the dissociation behavior of both coronas using Fourier Transform Infrared Spectroscopy. Lower pH region ($3.6 < pH < 5.0$) in aqueous medium offers stronger interactions between oppositely charged corona blocks, resulting in polymeric hexagonal prism complexes. In the higher pH region ($5.5 < pH < 6.5$), they first self-assembled into hierarchical bumpy spheres induced by the simple adsorption of small PS-b-PAA BCMs on the surfaces of PS-b-P4VP large compound micelles since the degree of ionization of P4VP blocks is relatively low. However, the crew-cut BCM complex morphology with high aggregation number does not allow the hexagonal prism structure to be formed without rearranging strongly aggregated core blocks. We note that the crew-cut BCM complexation in higher DMF content of a mixed solvent (1 % < DMF < 20 % in water) induces inter-corona association leading to the hexagonal prism structure due to the decrease in selectivity of water for PS blocks.

In the last chapter, we demonstrate the hierarchical structures of block copolymer blend,

mixture of PS-b-PAA and PS-b-P4VP, in various solvent qualities. P4VP & PAA homopolymers mixed in aqueous solution can be preferentially dissociated at specific solution pH region. That is, solution pH is approached to 1, P4VP can be preferentially charged. However, solution pH increase to 14, PAA can be preferentially dissociated. In addition, P4VP segments are soluble at solution pH < 5.5 since P4VP segments can be positively charged in the pH region. Based on this study, morphologies of PS-b-PAA and PS-b-P4VP blends were controlled by initial pH and solvent quality. As a result, when they are mixed together in co-solvent dominant environment, their phase can be separated similar in bulk. However, they are mixed in water-dominant solvent, their blend morphology are only vesicles at extremely high or low pH because their coronas are very sensitive to solution pH.

Keywords: polyelectrolyte, multilayer, complex, block copolymer micelle, block copolymer blend

Student Number: 2009-30246

Contents

CHAPTER I

Multilayer Deposition on Patterned Posts Using Alternating Polyelectrolyte Droplets in Microfluidic Devices

1.1. Introduction

The Layer-by-Layer (LbL) deposition, first introduced by Decher (*1*) in 1997, has been regarded as a simple and robust processing method to obtain various multilayered films typically on flat substrates. Based on the LbL deposition method, it has been well-documented that the functions and physical properties of the LbL films could be easily tailored (*2-7*). Multilayer thin films have recently attracted numerous interests owing to their wide applications as sensors, integrated optics, polymer electronic devices, drug delivery systems, or biocompatible scaffolds, which could be easily deposited and tailored on the substrates of different shape (*8-15*).

Over the past years, the LbL deposition technique, which has originally been based on the diffusive adsorption of polyelectrolytes (PEs) on a substrate without external convective driving forces, have evolved into alternative deposition methods such as the spin-assisted LbL deposition (*3, 16*), as well as the spray-based LbL deposition (*17, 18*). However, these conventional LbL deposition methods require four typical sequential steps: the adsorption of (+) PE followed by washing off with water (or solvent) and the adsorption of (-) PE followed by second wash-off for one full cycle, which typically takes long process time. In particular, the LbL film deposition on colloids (*19, 20*) is severely limited by the fact that it requires the

PE adsorption on colloids, centrifugation to remove unadsorbed PEs, and the sonication to redisperse the colloids so that the stability of colloids is not guaranteed after more than 10 repeated depositions of PE resulting from theseparation of colloids.

Since the advent of microfluidics about two decades ago, we have witnessed the explosive increase in the interest and development for fluid flows at the microscale, which could offer a lot of useful capabilities, which have not been possible before: the ability to use a very small quantity of samples and reagents, and to expand on existing unit operations such as separation, mixing, detection, chemical reaction and bioassay with high precision and sensitivity (*21-23*). Microfluidic systems are generally characterized by the low Reynolds number flow regime to create novel micro-environments (*24-26*), dictating that all fluid flows are essentially laminar. Droplet-based microfluidics, however, has the ability to perform a large number of reactions without increasing device size or complexity. These droplet-based microfluidic systems, coupled with the control capability and reproducibility of droplet generations, directly synthesize micro/nano-particles for applications such as drug delivery systems and microreactors ranging from nano to femtoliter range (*27-34*).

A few research groups have previously reported on the microfluidic multilayer preparation based on the laminar flow to alleviate the process time compared with the conventional deposition methods (*35, 36*). In the dynamic LbL deposition system suggested by Kim et al., PE and washing streams had to be separately introduced into the channel for the sequential adsorption of PEs, similar to the spin-assisted LbL deposition. In the microfluidic channels designed by Caruso et al., the channel geometry for the deposition of a single bilayer had tobe increased in proportion to the number of bilayers, which severely limits the applicability of this deposition method. Since the previous microfluidics-based LbL depositions were basically based on the single-phase system, we strongly believe that there would be

significant improvements in the LbL deposition, in terms of process time, the amount of adsorbents (such as PEs) consumed, design flexibility, and saving energy, using microfluidics if a droplet-based two-phase microfluidic system is employed.

Here, we demonstrate the droplet-based LbL deposition with which PE multilayers deposited on patterned post(s) with incredibly large numbers of bilayers, which cannot be possibly obtained with the conventional deposition methods, could be obtained in short process time using a simple two-phase microfluidic channel. In addition, the impaction of droplets onto small targets has recently been investigated (*37-40*) and simulated (*41, 42*), which were quite different from the impact of a small droplet onto a large object (*43*). Since the target substrate can be generated by the optofluidic maskless lithography (OFML) technique (*44, 45*) at a specified position with any geometric shape within the microfluidic channel, the experiments demonstrated in the present study could serve as a model system to study the droplet dynamics for impacting of small droplets on various obstacle patterns in addition to totally new microfluidics-based LbL deposition. From the perspective of adsorption kinetics, the microfluidic device introduced here could also provide a studying tool for the contact time in millisecond scale, which would not be accessible in earlier experimental techniques.

1.2. Experimental Section

Fabrication of a Cross-shaped Microfluidic Channel and Materials Used

The microfluidic channel used for the present study was fabricated using the standard soft lithography method (*46, 47*). PDMS molds were fabricated by curing PDMS pre-polymer (Sylgard 184 Silicon elastomer, Dow Corning) and sealed with a slide glass using O_2 plasma treatment for 45 sec (60 W, PDC-32G, Harrick Scientific). The main flow channel is 200 μm wide, 40 μm deep, and 2 cm long.

PAH (poly(allylamine hydrochloride), Mw = 15,000) and PSS (poly(sodium 4-styrenesulfonate), Mw = 70,000) used for two different aqueous polyelectrolyte (PE) streams, were purchased from Sigma Aldrich. All the polyelectrolyte aqueous solutions were used without pH adjustment as well as the addition of ionic salt in this study. FITC (fluorescein isothiocyanate)-labeled PAH (PAH-FITC) was synthesized by following the modified procedure from the previous work (*46*): 1 g of PAH was dissolved in 20 mL water with pH adjusted to 9. The solution was mixed with 150 mL of methanol and the solution temperature was maintained between 0 and 4 °C under vigorous stirring. 1 mL of concentrated FITC solution (41 mg in 1 mL DMF, which is 1/100 equivalent to the PAH repeat unit concentration) was prepared and added dropwise to the mixture. The mixture was shielded from sunlight by wrapping the flask with aluminum foil and allowed to react at 4 °C overnight. The labeled polymer (PAH-FITC) was then purified by repeated precipitation with DMF followed by dialysis until no fluorescence was detectable in the washing solution. The dialyzed polymer solution was freeze-dried. The yield of the labeling reaction or the labeling ratio was determined by UV-Vis. spectroscopy (Perkin Elmer Lamda 35). Absorption and

emission peaks of FITC-labeled PAH were almost the same as the peaks for a dilute FITC solution, implying that there is virtually negligible interactions among dyes attached along the PAH chain.

We controlled the volumetric flow rate through each inlet channel using a syringe pump. PEs and oleic acid (Sigma Aldrich), used as a continuous phase in the present study, were pumped using 500 μL (1700 series, Needle type) and 2.5 mL (1000 series, Needle type) Hamilton Gastight syringes, respectively. The syringes were connected to the microfluidic channel with Tygon Teflon tubings (30 gauge). Syringe pumps from Harvard Apparatus (PHD 22/2000 Infusion/withdraw pumps) were employed in the infusion mode to feed both aqueous solutions and oil continuous phase into the channel inlets.

The viscosity of the carrying fluid (oleic acid) is 27.64 mPa s measured by a Strain Controlled Rheometer (ARES, TA instrument). Also, the interfacial tension between the aqueous dispersed phase and the continuous phase is 15.6 g s^{-2}, as measured by a Surface Tensiomat 21 (Fisher Scientific). Based on these measured values, we calculated the flow rate of the continuous phase in the designated Ca region. Aqueous PE droplets generated from the inlet channels were observed at 8000 fps by a high-speed video camera (FASTCAM ultim 512, Photron, Japan).

Formation of Patterned Posts Using OptofluidicMaskless Lithography

We used poly(ethylene glycol) diacrylate (PEG-DA, Sigma-Aldrich, Mn = 258) with 5 wt% of photoinitiator (2,2-dimethoxy-2-phenylacetophenone) to create patterned posts inside the microfluidic channel. Patterned posts, used as substrates for the LbL assembly with PE droplets, were formed by the crosslinking of PEG-DA with UV light based on the optofluidicmaskless lithography (*44*). An oligomeric solution containing PEG-DA and

photoinitiator was first injected into the microfluidic channel. The UV light pattern generated by optofluidicmaskless lithography system (OFML) was shined on the microfluidic channel filled with the oligomeric solution. The area in the oligomeric solution, under which UV light was illuminated, was polymerized within 0.4 ~ 0.5 sec. By controlling the shape and location of UV light pattern with the aid of PC Program control (Labview), we were able to prepare polymeric posts with two different shapes at desired positions in the microfluidic channel. The PEGDA posts of 100 μm in diameter were also accurately attached at the bottom of the channel such that the centerlines of droplets are well aligned with the centerline of the posts.

Measurement of Fluorescence Intensity of LbL Multilayer Films Deposited on the Posts

Fluorescent micrographs of the LbL films deposited on the posts were taken with an Olympus IX71 optical microscope with a wide-excitation green filter set (11007v2). The angle-averaged fluorescence intensity as well as the surface intensity plots was obtained from these fluorescent microscopic images using an image analysis program (Image Pro).

1.3. Results and Discussion

To demonstrate the continuous generation of alternating droplets, a cross-shaped microfluidic geometry with three inlets and one outlet was prepared, as shown in Figure 1(a). Two different polyelectrolytes (PEs), of which the chemical structures are shown in Figure 1(b), for the multilayer deposition are dissolved within alternating droplets through the two capillary inlets connected to the main channel. Two different PE droplets are then carried by a continuous carrier fluid (i.e., oleic acid in the present study) to allow those droplets to pass around the patterned micro-post(s).

The patterned post, serving as a substrate for the PE deposition, is generated with a photo-curable polymer, PEGDA (poly(ethylene glycol) diacrylate), in the microfluidic channel based on the optofluidicmaskless lithography (*44*). Isolated micro-posts of any size and shape can be generated by this patterning method and fixed to the bottom centerline for the precise contact with PE droplets.

To monitor the multilayer deposition, we chose a layer-by-layer (LbL) multilayer assembly pair based on the Coulombic interaction between positively-charged PAH (poly(allylamine hydrochloride)) labeled with FITC (fluorescein isothiocyanate) and negatively-charged PSS (poly(sodium 4-styrenesulfonate)) (Figure 1(b)). The green fluorescence dye, FITC, has the absorption maximum at 494 nm and the emission maximum at 521 nm in aqueous solution.

To realize the microfluidic LbL deposition, we mainly focused on two parameters to generate alternating dropletsand to control the droplet generation frequency: capillary number (Ca) and flow rate fraction (R_f). The capillary number, Ca, represents a measure of the viscous stress relative to the interfacial tension stress46, $Ca = \mu U \gamma^{-1}$, where U ($m\ s^{-1}$) is the flow

velocity, μ (kg m^{-1} s^{-1}) is the dynamic viscosity, and γ (kg s^{-2}) is the interfacial tension between the dispersed PE phase and the continuous oil phase. It has been reported that the capillary number (Ca) is the key parameter to control the size and generation frequency of alternating droplets. Since the droplet size is mainly controlled by the width at the pinch junction while Ca only slightly affects the size, a minor change in Ca would not significantly alter the droplet size in the present study. Several research groups have shown that the optimal Ca range for the successful alternating droplet generation, without neighboring droplets touching each other, lies in $0.001 < Ca < 0.15$ (*48-50*). The lower limit of the Ca range ($0.001 < Ca < 0.051$) is particularly interesting in the present case for the droplet-based LbL deposition since the droplets generated in this regime are plugs, with the droplet diameter larger than the cross-sectional dimension of a mircofluidic channel, capable of full contacts with a patterned post. With the known viscosity for each phase (water droplet or oil phase) and the interfacial tension between the oil and PE phases, we were able to generate the plug-shaped droplets by simply controlling the flow rate of a continuous phase ranging from 0.2 ~ 13.8 μL min^{-1}.

The flow rate fraction (R_f) is defined as the ratio between the flow rate (μL min^{-1}) of PE droplets to the sum of flow rates (μL min^{-1}) of both oil and PE phase. It has been demonstrated that R_f is the key parameter to control the spacing between droplets, alternating droplet ratio, and droplet size at a fixed Ca. For example, the spacing between droplets decreases and the droplet size increases with the increase in R_f (*50-52*). In addition, by varying the relative flow rate in the two different PE inlet channels, the mircofluidic device allows the generation of alternating droplets with different droplet ratio (*48*). The lower limit

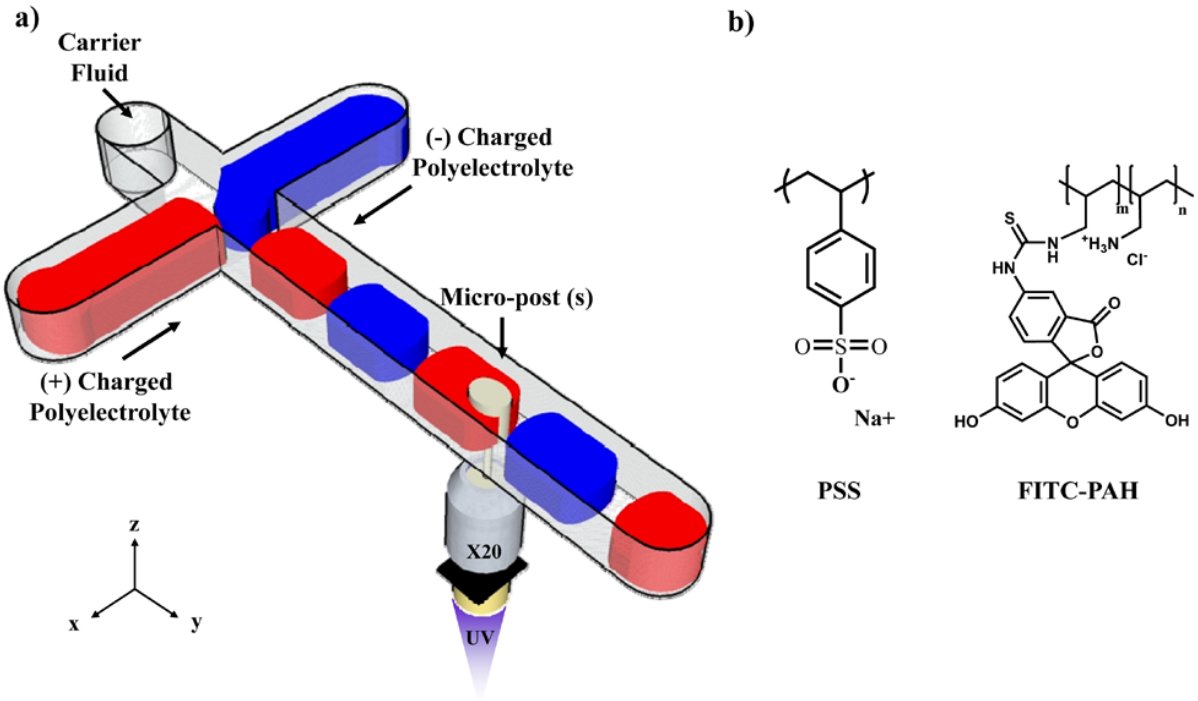

Fig.1 (a) A schematic on the microfluidic device for the layer-by-layer (LbL) deposition on a pattered post coupled with optofluidicmaskless lithography; (b) polyelectrolytes used for the LbL droplet deposition in this study.

in R_f value (< 0.4) is particularly useful in the present case to secure enough spacing between droplets (*48, 50-52*). Since the positively- and negatively-charged PE droplets can easily aggregate together when those two droplets touch each other owing to the attractive electrostatic interaction. For this reason, we fixed the value of R_f at 0.2.With these experimental conditions worked out, we obtained fluorescence microscopic images in Figure 2(a), showing alternating droplets at different time frames with two PE streams: a colorless PE droplet (PSS) and a green fluorescent PE droplet (FITC-PAH). In good agreement with the previous observations, a FITC-PAH droplet is growing at the double T-junction and finally pinched off at the corner easily (*48-50*). The changes in drop pair (PSS and FITC-PAH droplets) frequency (ω_d in pairs per second (pps)) and contact time of a single droplet (in milliseconds (ms)) as a function of Ca are shown in Figure 2(b). We note that the droplet pair frequency increases from 5 to 102 pps while the contact time of a single droplet, estimated by the measured number of frames obtained from the droplet movement captured by a high speed camera, decreases from 55 to 2.5 ms with increasing Ca. We also note that the measured contact time of a single droplet passing the post is in good agreement with the simple estimation of the droplet contact time based on the volume of a single droplet at a given Ca number. It is important to note at this stage that one complete cycle for a bilayer deposition on a patterned post consists of four different steps: consecutive flows with a positively charged polyelectrolyte droplet (i.e., adsorption of positively charged PE on the patterned post), continuous medium (i.e., washing off physically adsorbed PE chains), a negatively charged polyelectrolyte droplet (i.e., adsorption of negatively charged PE), and continuous medium (i.e., washing off physically adsorbed PE chains). For the multilayer deposition, this complete cycle can be repeated as many as desirable. In order to confirm the

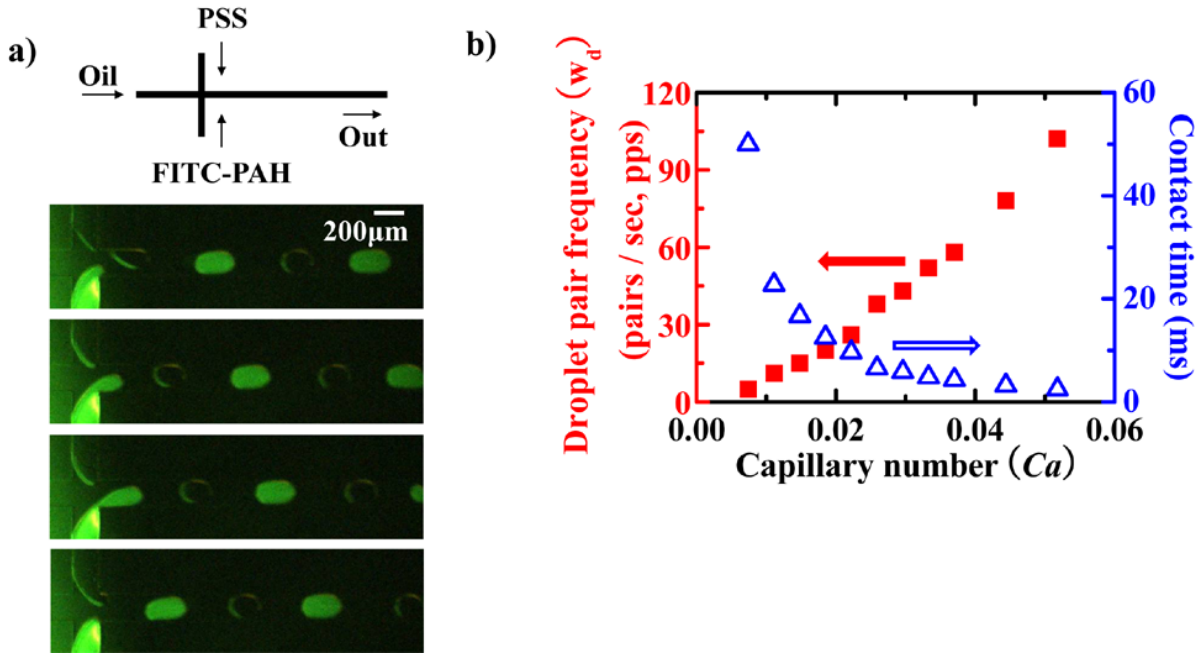

Fig.2 (a) A schematic illustration of the experimental setup for generating alternating droplets (upper) and the fluorescence microscopy images showing the formation of alternating droplets (lower); (b) the droplet pair generation frequency (ω_d) and the contact time of a single droplet plotted against the capillary number (Ca).

effect of capillary number (Ca), we chose two different values of Ca: 0.007 and 0.022. Figure 3(a) shows that the droplet pair frequency with Ca = 0.022 is found to be five times higher than the value with Ca = 0.007. We also notice that the droplet volume (~ 1 nL) generated with Ca = 0.022 is smaller than the droplet volume (~ 1.67 nL) createdwith Ca = 0.007 but with the droplet size still larger than the cross-sectional dimension of the fluidic channel, thus generating plug-shaped droplets. We also confirm that the droplets generated with both Ca values do not touch each other, staying as separate droplets during the movement in the microfluidic channel.

In order to assess the Ca effect on the PE deposition on a patterned post, we obtained the angle-averaged fluorescence intensity as a function of droplet pair number for two different Ca values, as represented in Figure 3(b). The number of droplet pairs that collide on the patterned post for the LbL deposition is estimated by the multiplication of the droplet generation frequency with deposition time. Figure 3(b) shows the almost linear relationship between the fluorescence intensity, which is, in turn, related to the amount of FITC-PAH adsorbed onto the patterned post, and the droplet pair number in the range tested in the present study for two different Ca values. It is interesting to note that the adsorbed amount, as inferred from the fluorescence intensity, is much higher with a lower Ca value at a given droplet pair number. This is due to the fact that the average contact time of a droplet pair on the post for PE adsorption is much longer with smaller Ca value. As noted by Kim and coworkers, the LbL deposition at the bottom surface of a fluidic channel based on the laminar flow could safely neglect the possible desorption of PEs with typically large adsorption constants and thus the larger adsorbed amount of PEs with the current case of droplet-based LbL deposition could be achieved in comparison with the conventional LbL deposition methods. They also mentioned that the contact time, not the flow rate, actually affects the

bilayer thickness in the two regimes: equilibrium and nonequilibrium conditions, which are proven to be applicable in the current case of droplet-based LbL deposition.(*35*) In our present case, we could even extend the LbL adsorption analysis down to the millisecond contact time with nanoliter volume of PE droplets. To conform this, we varied the contact time per droplet pair by changing the value of Ca as shown in Figure 3(b). It is shown that the fluorescence intensity of PEs adsorbed with a lower Ca and, at the same time, longer contact time is higher than the intensity at a higher Ca with shorter contact time. Consequently, we obtained the fluorescence contour plot around a patterned post adsorbed with 60k droplet pairs for two different Ca values, shown in Figure 3(c). In addition, we note that when we have used 50 μL of PE solution in each PE phase, which translates into the fact that 30k droplets are allowed to deposit with Ca= 0.007 while 50k droplets are allowed to pass the post for adsorption with Ca = 0.022, we found that the fluorescence intensity of PEs adsorbed with both Ca values is about the same, implying that the flow rate itself does not affect the adsorbed amount of PEs even in the millisecond contact time.

It is also worthwhile to note that the fluorescence data presented on the left side of a plot in Figure 3(b) is not easily experimentally accessible, implying that weak fluorescence intensity, just detectable from zero intensity, is obtained with mere 200 μL of dilute PE solutions (10 mM) for 200 min of droplet impacts on the patterned post in the current microfluidic device. On the contrary, we found that the thickness of a PE film deposited with 60k droplets on the post was above 1 μm, as confirmed by both SEM and CLSM images (Fig. 4). The average estimate of bilayer thickness in the present case with the LbL deposition in a microfluidic channel is about 0.5 Å (1 μm / 60k droplets). We believe that such a low estimate of the

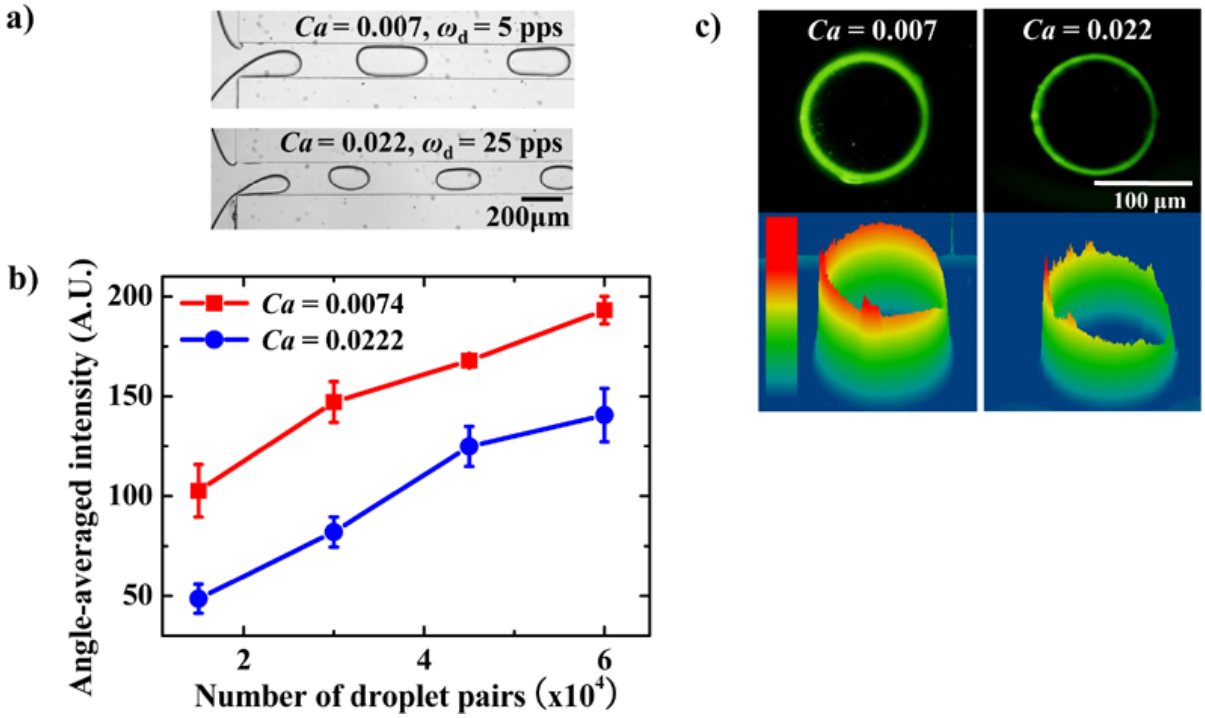

Fig.3 Monitoring of LbL film growth based on the increase in fluorescence intensity of (+)-charged PAH tagged with FITC dye deposited on a patterned post: (a) optical microscopic images show the droplets, captured by a high-speed video camera, at two different Ca's; (b) the angle-averaged fluorescence intensity plotted against the PE droplet pair number at two different Ca's; (c) plan-view fluorescence intensities (upper) and the surface plots of fluorescence intensity (lower) of 60k PE droplet pairs bumped on the post at two different Ca's (flow passes from left to right).

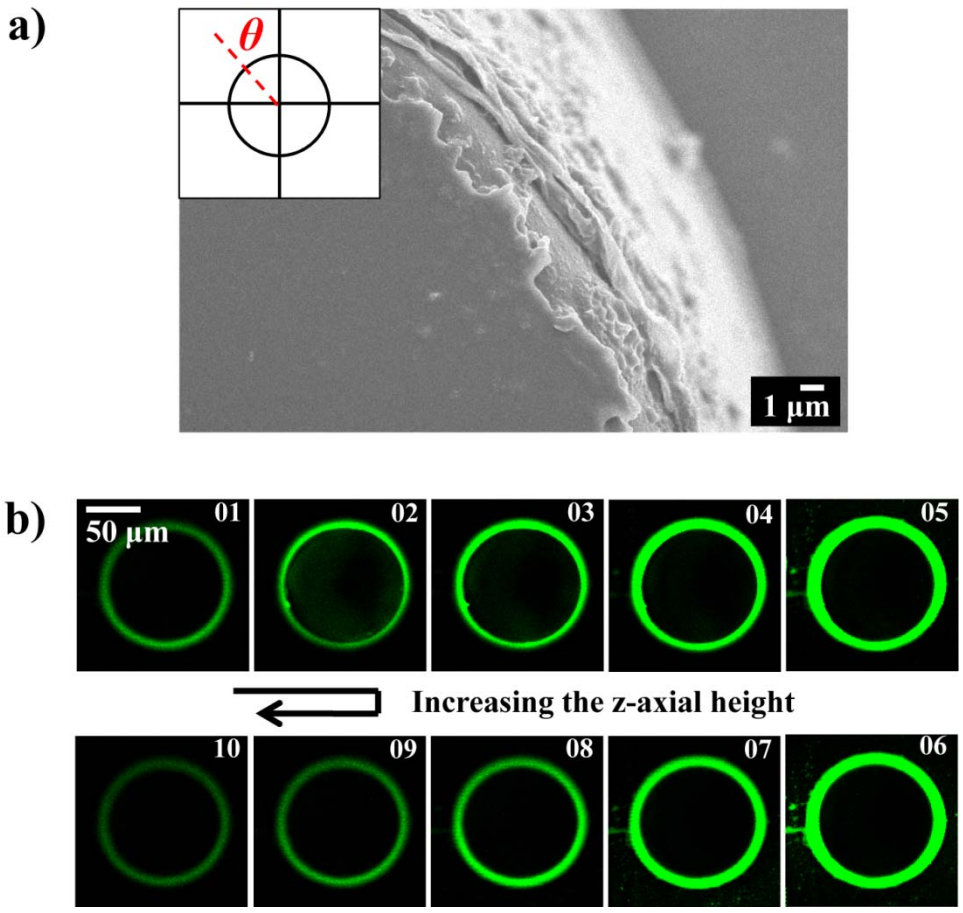

Fig.4. (a) A SEM image showing a cylindrical post, detached from the microfluidic substrate, containing PEs deposited by the droplet LbL assembly; (b) the CLSM images, taken from the bottom to the top of a patterned post in 10 slices, of PEs deposited onto the cylindrical post for 200 min at Ca = 0.007. (θ indicates the angular position in the post where the SEM picture was taken).

bilayer thickness in the current case is mainly due to the incomplete coverage of PEs on an isolated object during such a short contact time (10 ~ 55 ms). From flow visualization experiments, a single droplet (of volume 1 ~ 1.67 nL) covers the whole isolated object but the PE adsorption is not enough during such a short contact time.

This simple experiment leads us to the following four different perspectives in the present study: first, the bilayer film thicknesses achieved by spin-assisted LbL and dip-based LbL depositions with the same PE pair have been known to be around 24 and 4 Å, respectively, when the same molar concentrations of PEs were used.(*3*) Therefore, for the same process time, 200 min in the present case, both spin LbL, which usually takes ~ 3 min per bilayer deposition, and dip LbL, taking approximately 40 min per bilayer formation, yield much thinner bilayer thicknesses (i.e., ~ 160 nm and ~ 2 nm, respectively) in comparison with about 1 μm of film thickness achieved from the current droplet-based LbL deposition. Secondly, the amount of PE solutions consumed for the deposition of ~ 1 μm of PE film thickness was about 200 μL in the microfluidic device (i.e., 0.5 μL min-1 for 200 min with two kinds of PEs), which is much less than the volume required for the spin LbL (~ 1 mL/bilayer required) and the dip LbL (~ 20 mL/bilayer required) to achieve the same PE film thickness on a substrate. Thirdly, the droplet-based LbL in a microfluidic device can serve as an important experimental tool to study the effect of adsorption kinetics on the LbL deposition. Finally, the droplet deformation dynamics occurring from the impact of a droplet on a patterned micro-post can be experimentally investigated in this microfluidic device, as demonstrated in Figure 5 & 6.

Flow pattern around a patterned obstacle, in general, depends on the shape of the obstacle and overall flow conditions.(*53*) Particularly, the drop impact and spreading onto a curved

substrate are strongly influenced by the geometry of the obstacle whose radius of curvature is smaller than the PEs dissolved in droplets in our microfluidic device, we prepared two different patterned posts, as shown in Figure 5& 6. The conical post is slightly modified from the cylindrical post in the back region of a cylinder to make it more suitable for a streamlined flow.

We experimentally observed the droplet flows around patterned posts after the impact on a cylindrical or a cone-shaped micro-post, captured by a high speed camera, with Ca = 0.007 in Figures 6(a) and 6(d), respectively. A PE droplet is initially divided into two equal parts due to the presence of a center-positioned post. It is also noted that the divided droplet portions are not merged together in the rear region of the post. In the case of the conical post, PE droplets almost entirely contact the whole post including the back region, unlike the droplet flow around a cylindrical post. Experimental results are presented in the form of the distribution of adsorbed PEs (i.e., fluorescence intensity from adsorbed FITC-PAH) around the post taken at different time frames after the impact of droplet on the post (Figures 6(c) and 6(f)).

To justify the experimental measurements, we also present simulation results on the single phase flow near an obstacle (Fig. 5). Figures 6(b) and 6(e) show the streamlines and pressure contours near a cylinder and a conical obstacle, respectively. The pressure in the figure is normalized with $\mu U/(0.5\omega)$, where ω is the channel width. These simulation results would be able to help us understand the spatial variation of contact area of a droplet around a post,obtained from the experiment on the droplet flow around a patterned post. In other words, the PE droplets are carried by the continuous flow and the spatial variation of PEs adsorbed

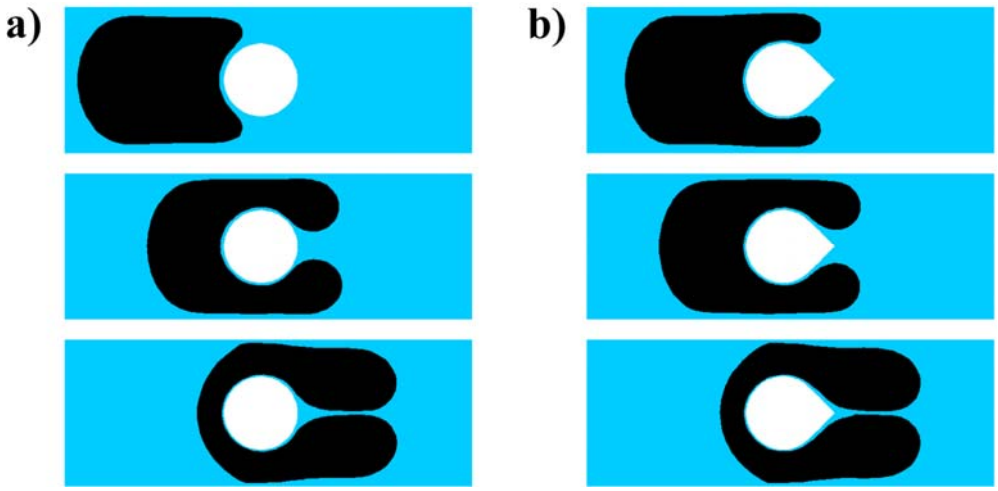

Fig5. Simulation results on the droplet movement around a post at Ca = 0.05 with dimensionless droplet length (α_d) = 1.3 (the dimensionless drop length (α_d) is defined as the ratio between the lateral drop length to the channel width), the viscosity ratio between droplet and medium = 1/30, mesh size (Δx_{max} / w) is 0.05: (a) cylindrical post; (b) conical post.

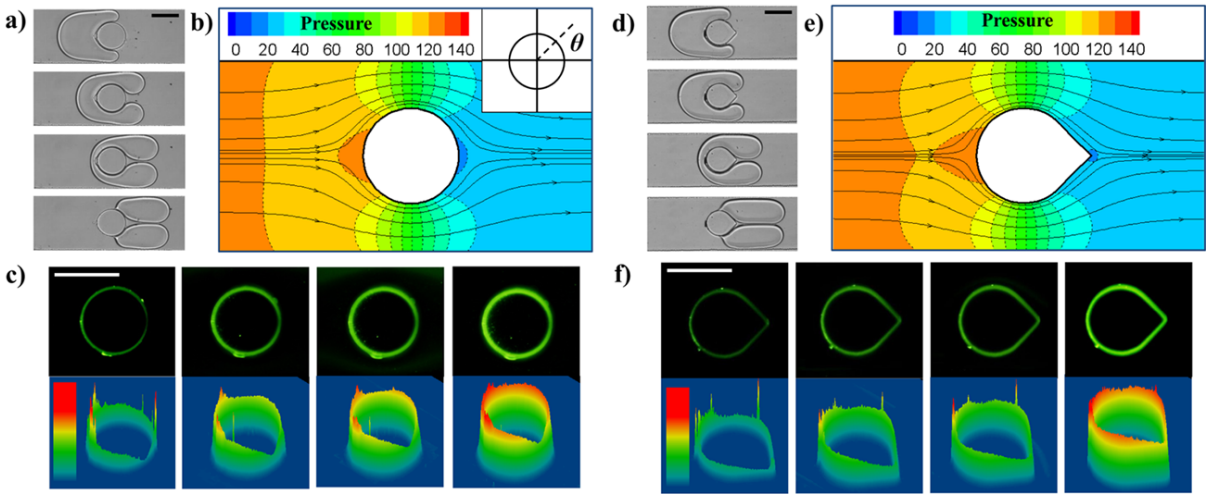

Fig.6 The comparison of experimental data (a, c, d, and f) with simulation results (b and e) for two different shapes of patterned posts: (a) ~ (c) for a cylindrical post and (d) ~ (f) for a conical post. For the experimental data, droplet motions, captured by a high speed camera, around each post are shown in (a) and (d), respectively; the plan-view fluorescence intensity as well as the surface intensity plot (image rotated at - 40^{o}) is shown in (c) and (f)) at different deposition times (50, 100, 150 and 200 min). For the simulation results, streamlines and pressure distributions are shown in (b) and (e) for two different shapes of patterned posts (All the scale bars shown in the figures are 100 μm).

onto the post is assumed to arise from the contact of such PE droplets, which are, in turn, carried by the continuous phase. We note that the streamlines around the conical post, shown in Figure 6(e), are uniformly formed closer to the boundary of the post, particularly at the east pole.

We also try to gain insight on the droplet flow dynamics by identifying the distribution of PEs, initially dissolved in droplets, adsorbed onto a patterned post. The angle-resolved fluorescence intensity from the adsorbed PE (FITC-PAH) increases with droplet deposition time or the number of droplet pairs impacting on the post. Note that these fluorescent microscope images shown in Figures 6(c) and 6(f) were obtained with keeping the contrast and brightness fixed. In the case of a cylindrical post, the fluorescence intensity of PEs adsorbed in the back region of the post is much lower than the intensity from the rest of the post during the entire deposition time (Figure 6(c)). However, in the case of a conical post, fluorescently labeled PEs are more or less uniformly adsorbed around the post including the back region (Figure 6(f)). Consequently, the experimental results on the variation of PEs adsorbed onto patterned posts reveal important relationship between the dynamics of droplets impacting on a post and the shape of the post.

We have also investigated the effect of the spacing between neighboring posts on the deposition of PEs from droplets passing around the posts. To this end, we prepared microchannels containing two cylinder post (with a diameter of 100 μm) arrays with two different spacings between the two cylindrical posts. The two cylindrical posts are 200 and 150 μm apart in the center-to-center distance oriented in the flow direction, as depicted in Figure 7.

To verify the droplet flow around dual posts, we also conducted numerical simulations on the

Newtonian flow around dual posts showing the velocity field as well as the streamlines around the dual posts, shown in Figures 7(a) and 7(e) for two different spacings between the posts. The streamlines around the dual posts with a spacing of 200 μm are shown in Figure 7(a), suggesting that an incoming droplet would be able to penetrate deep enough into the centerline between the two posts in the case of $l_i \sim \omega$, where li is the distance between the centers of two posts and ω is the channel width. In contrast, the streamlines are not fully developed in the interval between the dual posts in the case of $l_i = 0.75\ \omega$ with a spacing of 150 μm between the two posts. In other words, the lowest velocity region, color-coded with blue in Figure 7(e), in the case of $l_i = 0.75\ \omega$, is much thicker in comparison with the velocity field derived from $l_i \sim \omega$.

In order to compare with the simulation results involving the flows around dual posts, we allowed PE droplets to pass around the dual posts as shown in figure 7(b), (f) and obtained fluorescent microscopy images on fluorescently labeled PE adsorbed onto both posts as shown in Figures 7(c) and 7(g). Based on these images, we analyzed the PE adsorption site on each post in the dual posts based on the angle-resolved intensity plot, shown in Figures 7(d) and 7(h). These angle-resolved intensity plots show good qualitative agreement with the simulation data based on the streamlines and velocity field. In the case of $l_i \sim \omega$ (with a larger spacing between the two posts shown in Figures 7(c) and 7(d)), the angle-resolved intensity patterns for both posts are nearly identical to the intensity distribution on a single post. The fluorescence intensity of PEs adsorbed near the east pole of the post (corresponding to $\theta = 0$) shows the lowest value. This implies that the spacing between the two posts, equivalent to the channel width, is sufficient enough to behave like the droplet flow around an isolated post. However, when the spacing between the two posts is close enough as shown in Figure 7(g),the adsorption of PE in the head region of the second post (i.e., the west pole, $\theta = 180$) is

hindered as well as the back regions of both posts. The distribution of PEs adsorbed onto both posts is also shown in the angle-resolved intensity plot shown in Figure 7(h), which is again in good agreement with the simulation results. We can thus conclude that the minimum spacing between the centers of two posts to realize the droplet-based LbL deposition of PEs on a single post would be equivalent to the channel width at low Ca in the current experimental condition. Since all the numerical simulations conducted in the present study were based on the dimensionless variables such as the post size (1/2; fixed) and the distance (l_i ~ either 1 or 0.75) between the two posts normalized by channel width (ω), the experimental results presented here would also be valid in other scaled dimension as far as the PE droplet shape remains as plugs, as mentioned earlier.

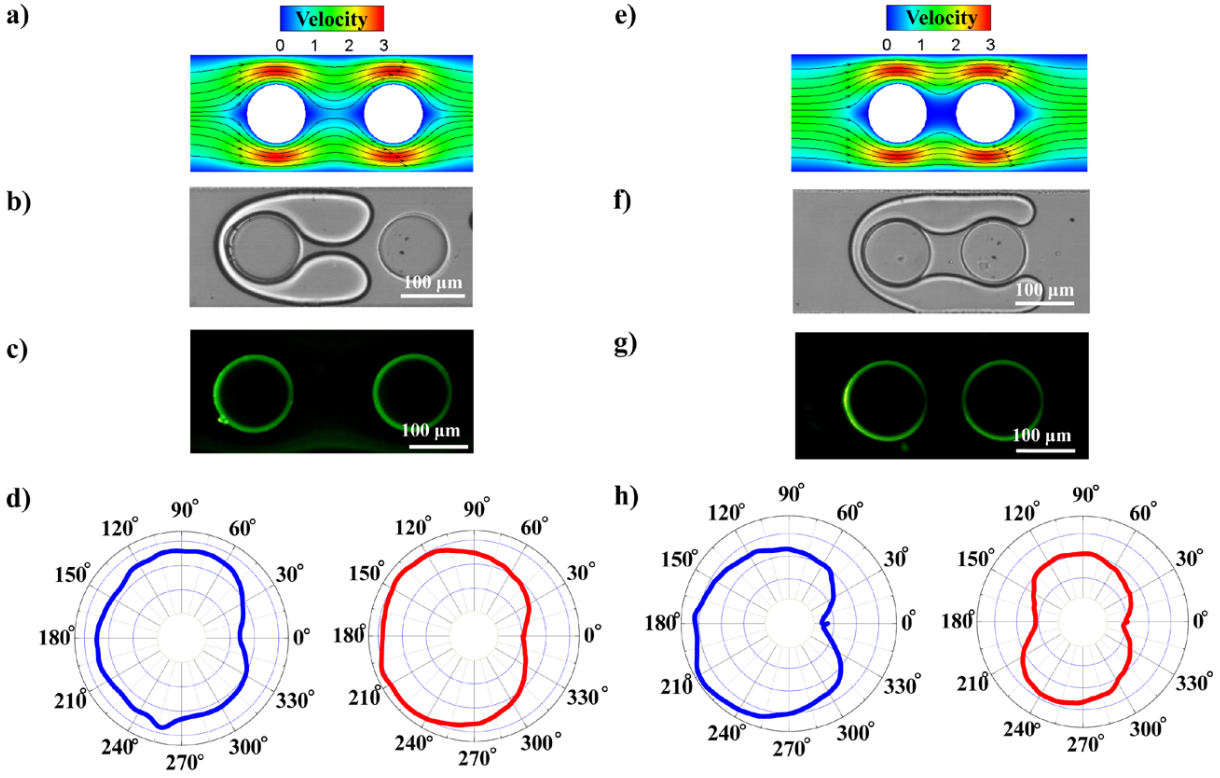

Fig.7 The comparison of simulation results (a and e) with experimental data (b, c, d, f, g, and h) for the LbL droplet deposition on two aligned cylindrical posts as a function of the distance (l_i) between the centers of the two posts: (a) ~ (d) for l_i = 1.0 ω and (e) ~ (h) for l_i = 0.75 ω where ω is the channel width. The velocity field and streamlines around the dual aligned posts are shown in the simulation results (a and e). The angular fluorescence intensity plot (d and h) were obtained from the fluorescence images (c and g) of PEs deposited with 20k droplet pairs passing around the dual posts (b and f: images captured with high speed camera) at Ca = 0.007.

1.4. Conclusion

We demonstrated that polyelectrolyte (PE) multilayer thin films deposited on patterned posts flowing with numerous alternating PE ((+)- and (–)- charged) droplets can be achieved in short process time in a microfluidic channel with 3 inlets and 1 outlet. All the experimental parameters, such as Capillary number (Ca) and flow rate fraction (R_f), to realize the alternating PE droplets as well as to control the droplet frequency and the spacing between the two different PE droplets have been worked out. The flow of alternating PE droplets around patterned posts enabled the alternating adsorption of PEs, similar to the layer-by-layer (LbL) deposition in bulk solution. The droplet-based LbL deposition shows the almost linear relationship between the amount of FITC-PAH adsorbed on the patterned post and the droplet pair number, showing a trend similar to the bulk LbL deposition but with much higher efficiency. We also investigated the effect of post shape, showing that the conical post is better for the uniform PE deposition compared with the cylindrical post. When the PE droplet flow around dual posts was examined, the minimum spacing between the centers of two posts to realize the droplet-based LbL deposition of PEs on a single post would be equivalent to the channel width, which is in good agreement with the numerical simulations and can also be readily scaled to other dimensions.

The droplet-based LbL deposition in a microfluidic channel could be extended to further applications. For example, the LbL deposition with alternating droplets on isolated objects, which could be patterned and locked is followed by the release and sorting of the PEG hydrogels with (functional) multilayers on the surface in the downstream of a microfluidic channel for additional applications. The lock-and-release of isolated patterned objects could be possible with the several methods suggested in the literature: one is the lock-release

lithography(*54*) and the other would be the lock-and-release with techniques such as optical tweezers or under magnetic field.(*55*)We believe that the recognition of isolated objects with different shape and charge would self-assemble into a supra structure for further applications.

1.5. References

1. G. Decher, Fuzzy nanoassemblies: Toward layered polymeric multicomposites. *Science* **277**, 1232 (Aug 29, 1997).
2. F. Caruso, R. A. Caruso, H. Mohwald, Nanoengineering of inorganic and hybrid hollow spheres by colloidal templating. *Science* **282**, 1111 (Nov 6, 1998).
3. J. Cho, K. Char, J. D. Hong, K. B. Lee, Fabrication of highly ordered multilayer films using a spin self-assembly method. *Adv. Mater.* **13**, 1076 (Jul 18, 2001).
4. J. Hiller, J. D. Mendelsohn, M. F. Rubner, Reversibly erasable nanoporous anti-reflection coatings from polyelectrolyte multilayers. *Nat. Mater.* **1**, 59 (Sep, 2002).
5. S. Markutsya, C. Y. Jiang, Y. Pikus, V. V. Tsukruk, Freely suspended layer-by-layer nanomembranes: Testing micromechanical properties. *Adv. Funct. Mater.* **15**, 771 (May, 2005).
6. K. T. Nam *et al.*, Virus-enabled synthesis and assembly of nanowires for lithium ion battery electrodes. *Science* **312**, 885 (May 12, 2006).
7. P. Podsiadlo *et al.*, Ultrastrong and stiff layered polymer nanocomposites. *Science* **318**, 80 (Oct 5, 2007).
8. Y. He, S. Gong, R. Hattori, J. Kanicki, High performance organic polymer light-emitting heterostructure devices. *Appl. Phys. Lett.* **74**, 2265 (Apr, 1999).
9. P. K. H. Ho *et al.*, Molecular-scale interface engineering for polymer light-emitting diodes. *Nature* **404**, 481 (2000).
10. A. Laschewsky, E. Wischerhoff, M. Kauranen, A. Persoons, Polyelectrolyte multilayer assemblies containing nonlinear optical dyes. *Macromolecules* **30**, 8304 (Dec, 1997).
11. J. D. Mendelsohn *et al.*, Fabrication of microporous thin films from polyelectrolyte multilayers. *Langmuir* **16**, 5017 (May, 2000).
12. Z. Y. Tang, Y. Wang, P. Podsiadlo, N. A. Kotov, Biomedical applications of layer-by-layer assembly: From biomimetics to tissue engineering (vol 18, pg 3203, 2006). *Adv. Mater.* **19**,

906 (Apr 6, 2007).

13. K. C. Wood, H. F. Chuang, R. D. Batten, D. M. Lynn, P. T. Hammond, Controlling interlayer diffusion to achieve sustained, multiagent delivery from layer-by-layer thin films. *Proc. Natl. Acad. Sci. U. S. A.* **103**, 10207 (Jul 5, 2006).

14. X. Zhang, J. C. Shen, Self-assembled ultrathin films: From layered nanoarchitectures to functional assemblies. *Adv. Mater.* **11**, 1139 (Sep, 1999).

15. K. C. Krogman, J. L. Lowery, N. S. Zacharia, G. C. Rutledge, P. T. Hammond, Spraying asymmetry into functional membranes layer-by-layer. *Nat Mater* **8**, 512 (06//print, 2009).

16. P. A. Chiarelli *et al.*, Controlled Fabrication of Polyelectrolyte Multilayer Thin Films Using Spin-Assembly. *Adv. Mater.* **13**, 1167 (2001).

17. C. H. Porcel *et al.*, Ultrathin Coatings and (Poly(glutamic acid)/Polyallylamine) Films Deposited by Continuous and Simultaneous Spraying. *Langmuir* **21**, 800 (2004).

18. J. B. Schlenoff, S. T. Dubas, T. Farhat, Sprayed Polyelectrolyte Multilayers. *Langmuir* **16**, 9968 (2000).

19. E. Donath, G. B. Sukhorukov, F. Caruso, S. A. Davis, H. Mohwald, Novel hollow polymer shells by colloid-templated assembly of polyelectrolytes. *Angew. Chem.-Int. Edit.* **37**, 2202 (Aug 17, 1998).

20. J. Hong *et al.*, Tunable superhydrophobic and optical properties of colloidal films coated with mock copolymer micelles/micelle multilayers. *Adv. Mater.* **19**, 4364 (Dec 17, 2007).

21. A. J. deMello, Control and detection of chemical reactions in microfluidic systems. *Nature* **442**, 394 (Jul, 2006).

22. P. S. Dittrich, A. Manz, Lab-on-a-chip: microfluidics in drug discovery. *Nat. Rev. Drug Discov.* **5**, 210 (Mar, 2006).

23. A. Manz *et al.*, Planar chips technology for miniaturization and integration of separation techniques into monitoring systems : Capillary electrophoresis on a chip. *J. Chromatogr. A* **593**, 253 (1992).

24. A. Hatch *et al.*, A rapid diffusion immunoassay in a T-sensor. *Nat. Biotechnol.* **19**, 461 (2001).

25. N. L. Jeon *et al.*, Neutrophil chemotaxis in linear and complex gradients of interleukin-8 formed in a microfabricated device. *Nat. Biotechnol.* **20**, 826 (Aug, 2002).

26. E. M. Lucchetta, J. H. Lee, L. A. Fu, N. H. Patel, R. F. Ismagilov, Dynamics of Drosophila embryonic patterning network perturbed in space and time using microfluidics. *Nature* **434**, 1134 (Apr 28, 2005).

27. T. H. Eun *et al.*, Single-Step Fabrication of Monodisperse TiO2 Hollow Spheres with Embedded Nanoparticles in Microfluidic Devices. *Chem. Mater.* **21**, 201 (Jan 27, 2009).

28. A. Gunther, M. Jhunjhunwala, M. Thalmann, M. A. Schmidt, K. F. Jensen, Micromixing of miscible liquids in segmented gas-liquid flow. *Langmuir* **21**, 1547 (Feb 15, 2005).

29. R. Karnik *et al.*, Nanomechanical control of cell rolling in two dimensions through surface Patterning of receptors. *Nano Lett.* **8**, 1153 (Apr, 2008).

30. S. A. Khan, K. F. Jensen, Microfluidic synthesis of titania shells on colloidal silica. *Adv. Mater.* **19**, 2556 (Sep 17, 2007).

31. D. Lee, D. A. Weitz, Double Emulsion-Templated Nanoparticle Colloidosomes with Selective Permeability. *Adv. Mater.* **20**, 3498 (2008).

32. Z. Nie, J. I. Park, W. Li, S. A. F. Bon, E. Kumacheva, An "Inside-Out" Microfluidic Approach to Monodisperse Emulsions Stabilized by Solid Particles. *J. Am. Chem. Soc.* **130**, 16508 (2008).

33. G. Schabas *et al.*, Formation and shear-induced processing of quantum dot colloidal assemblies in a multiphase microfluidic chip. *Langmuir* **24**, 10596 (Oct 7, 2008).

34. S. Y. Teh, R. Lin, L. H. Hung, A. P. Lee, Droplet microfluidics. *Lab Chip* **8**, 198 (2008).

35. H.-J. Kim, K. Lee, S. Kumar, J. Kim, Dynamic Sequential Layer-by-Layer Deposition Method for Fast and Region-Selective Multilayer Thin Film Fabrication. *Langmuir* **21**, 8532 (2005).

36. C. Priest *et al.*, Microfluidic polymer multilayer adsorption on liquid crystal droplets for

microcapsule synthesis. *Lab Chip* **8**, 2182 (2008).

37. Y. Hardalupas, A. M. K. P. Taylor, J. H. Wilkins, Experimental investigation of sub-millimetre droplet impingement on to spherical surfaces. *Int. J. Heat Fluid Flow* **20**, 477 (1999).

38. L. S. Hung, S. C. Yao, Experimental investigation of the impaction of water droplets on cylindrical objects. *Int. J. Multiphase Flow* **25**, 1545 (1999).

39. A. Rozhkov, B. Prunet-Foch, M. Vignes-Adler, Impact of water drops on small targets. *Phys. Fluids* **14**, 3485 (2002).

40. A. Rozhkov, B. Prunet-Foch, M. Vignes-Adler, Impact of drops of polymer solutions on small targets. *Phys. Fluids* **15**, 2006 (2003).

41. C. Chung, K. H. Ahn, S. J. Lee, Numerical study on the dynamics of droplet passing through a cylinder obstruction in confined microchannel flow. *J. Non-Newton. Fluid Mech.* **162**, 38 (2009).

42. C. Chung, M. A. Hulsen, J. M. Kim, K. H. Ahn, S. J. Lee, Numerical study on the effect of viscoelasticity on drop deformation in simple shear and 5:1:5 planar contraction/expansion microchannel. *J. Non-Newton. Fluid Mech.* **155**, 80 (2008).

43. S. Bakshi, I. V. Roisman, C. Tropea, Investigations on the impact of a drop onto a small spherical target. *Phys. Fluids* **19**, 032102 (2007).

44. S. E. Chung *et al.*, Optofluidic maskless lithography system for real-time synthesis of photopolymerized microstructures in microfluidic channels. *Appl. Phys. Lett.* **91**, 041106 (2007).

45. D. Dendukuri, D. C. Pregibon, J. Collins, T. A. Hatton, P. S. Doyle, Continuous-flow lithography for high-throughput microparticle synthesis. *Nat. Mater.* **5**, 365 (May, 2006).

46. G. Ibarz, L. Dahne, E. Donath, H. Mohwald, Smart micro- and nanocontainers for storage, transport, and release. *Adv. Mater.* **13**, 1324 (Sep 3, 2001).

47. J. C. McDonald *et al.*, Fabrication of microfluidic systems in poly(dimethylsiloxane). *Electrophoresis* **21**, 27 (Jan, 2000).

48. L. H. Hung *et al.*, Alternating droplet generation and controlled dynamic droplet fusion in microfluidic device for CdS nanoparticle synthesis. *Lab Chip* **6**, 174 (Feb, 2006).

49. T. Nisisako, S. Okushima, T. Torii, Controlled formulation of monodisperse double emulsions in a multiple-phase microfluidic system. *Soft Matter* **1**, 23 (2005).

50. B. Zheng, J. D. Tice, R. F. Ismagilov, Formation of droplets of in microfluidic channels alternating composition and applications to indexing of concentrations in droplet-based assays. *Anal. Chem.* **76**, 4977 (Sep 1, 2004).

51. S. Okushima, T. Nisisako, T. Torii, T. Higuchi, Controlled Production of Monodisperse Double Emulsions by Two-Step Droplet Breakup in Microfluidic Devices. *Langmuir* **20**, 9905 (2004).

52. T. Thorsen, R. W. Roberts, F. H. Arnold, S. R. Quake, Dynamic Pattern Formation in a Vesicle-Generating Microfluidic Device. *Phys. Rev. Lett.* **86**, 4163 (2001).

53. M. M. Denn, *Process Fluid Mechanics*. P. P. Hall, Ed., (Prentice-Hall, USA, 1939), pp. 383.

54. K. W. Bong, D. C. Pregibon, P. S. Doyle, Lock release lithography for 3D and composite microparticles. *Lab Chip* **9**, 863 (2009).

55. D. K. Hwang, D. Dendukuri, P. S. Doyle, Microfluidic-based synthesis of non-spherical magnetic hydrogel microparticles. *Lab Chip* **8**, 1640 (2008).

CHAPTER II

Janus-Type Multilayer Films with Block Copolymer Micelles in Microfluidic Reactors

2.1. Introduction

The applications of polymer-based drug delivery vehicles such as polymer particles, polymer-based micelles, polymer-drug conjugates, polymer capsules, and polymersomes have been investigated due to their great potential for the encapsulation and target delivery of water-insoluble biological materials (1-8). In recent years, Layer-by-Layer (LbL) assembly techniques have attracted considerable attention as accumulation methods for these drug delivery vehicles to satisfy requirements including compatibility with the targets, controlling the release profile of loaded materials, and increasing the loading amount of therapeutics (9-12). LbL assembly methods are known as simple and robust processing techniques for the sequential buildup of many kinds of desired nanomaterials into multilayered thin films (13-20). Since the introduction of dip-assisted diffusive adsorption of polyelectrolytes (PEs) by Decher in 1997 (21), alternative LbL deposition techniques have evolved deposition methods such as spin-assisted LbL deposition (22, 23), spray-based LbL deposition (24, 25), and microfluidic-based LbL deposition (26-28).

Over the past few years, block copolymer micelles (BCMs) have been used as novel nano-carriers for drug delivery systems. Their inner core region embedded with corona blocks can incorporate functional materials such as drugs, proteins, DNA, and personal care products

and the corona region can be modulated to exterior environments or stimuli (29, 30). Particularly, the corona region of BCMs can have a greater impact on their distribution in the body than the active material in the core (31, 32). In this respect, we can readily determine the distribution, targeting, and degradation of BCMs to address the requirements of practical drug carriers by controlling their surface properties.

Therefore, BCMs as nanoscale delivery vehicles with a unique interior-exterior structure accumulated within the multilayered thin films can be highly advantageous (9, 10, 33-36). However, multilayer films deposited on three-dimensional substrates using conventional deposition methods involving time-consuming processes such as centrifugation as well as redispersion cannot be extended to further delivery systems since the stability of colloids is not guaranteed after more than 10 repeated depositions of PE as a result of the separation of colloids (37, 38). In addition, conventional LbL deposition is not feasible for the accumulation of costly and limited-quantity biological reagents because the required amount of reagents consumed in conventional methods such as spin LbL and dip LbL is more than tens of milliliter per bilayer.

Therefore, in the present study, we demonstrate BCM/BCM multilayer thin films with a large number of bilayers by utilizing a nanoliter scale droplet-based deposition method in microfluidic channels. The BCM droplets alternately impact the patterned posts to induce the deposition of oppositely charged BCMs in a specific range of capillary numbers (Ca) of the continuous phase, resulting in BCM multilayer films with thicknesses of hundreds of nanometers requiring a small amount of BCM solution in a short process time. To date, the ability to deposit a large amount of BCMs onto colloidal substrates without a multi-step process involving steps such as centrifugation and redispersion by sonication has not been

possible.

Additionally, microfluidic channels including BCM-deposited posts can be utilized as an investigation tool for the in situ visualization of release behavior and optimization of shear-induced release conditions.

In conventional batch release systems, since materials released from substrates cannot be continuously removed, the total concentration in the closed system should be increased. Moreover, the release mechanism of the conventional system is only dependent on the diffusion of the medium being released into the multilayered films. Therefore, it is difficult to mimic the dynamic, three-dimensional microenvironment which is found in vivo. Conventional methods using a batch release system have been carried out which do not reflect in vivo dynamic conditions such as the shear stress caused by flowing blood. Both the three-dimensional environment and dynamic mechanical changes with realistic physiological setups are very important factors for the functioning of BCMs in drug release applications. As a result, it is beneficial to design microfluidic devices in a laboratory setup to allow researchers to consider these factors and control the relevant parameters.

In the present study, we first suggest a laminar flow system where it is possible to degrade the multilayer film deposited on microposts by providing a continuous and pristine release fluid. This approach offers great possibilities to closely mimic the physiological shear conditions in a fluidic setup for the systematic study of vascular cell biology in laboratories (body-on-a-chip system) (39-41). This microfluidic technology also permits precise control of the continuous degradation behavior of BCM multilayer films as functions of the exposure time and flow rate, leading to more comprehensive insight into drug delivery in vascular science. In addition, the volumetric ratio between two different releasing solvents in a microfluidic

channel can determine the contact areas of the BCM film to each releasing solvent, allowing their Janus degradation with a precise spatial resolution. Therefore, we can describe and observe a dual release system in a single channel, simultaneously investigating two different release kinetics and mechanisms induced by various external stimuli such as pH and shear, which are not accessible utilizing earlier experimental techniques.

2.2. Experimental Section

Fabrication of a cross-shaped microfluidic channel including a patterned post and preparation of the block copolymer micelles (BCMs)

The microfluidic channel used for the present study was fabricated using the standard soft lithography method (47, 48). The microfluidic channels were fabricated by curing polydimethylsiloxane (PDMS) pre-polymer (Sylgard 184 Silicon elastomer, Dow Corning) and sealed with a slide glass using O2 plasma treatment for 45 s (60 W, PDC-32G, Harrick Scientific). The main flow channel is 200 μm wide, 40 μm deep, and 2 cm long.

A micropost was formed by an optofluidicmaskless lithography system with poly(ethylene glycol) diacrylate (Sigma-Aldrich, Mn = 258), as we previously reported (26).

PS-b-P4VP (polystyrene-block-poly(4-vinylpyridine), Mw(PS) = 17,000, Mw(P4VP) = 49,000, PDI = 1.15) and PS-b-PAA (polystyrene-block-poly(acrylic acid), Mw(PS) = 16,000, Mw(PAA) = 4,000, PDI = 1.15) used for two different aqueous BCM streams were purchased from Polymer Source. The fluorescent dyes, Nile red (λex = 550 nm, λem = 610 nm) (10), pyrene (λex = 340 nm, λem = 396 nm) (10), and fluorescein isothiocyanate (FITC) (λex = 495 nm, λem = 521 nm) (26), were purchased from Sigma Aldrich and used for verification of the deposition and release of the BCMs.

For the preparation of protonated PS-b-P4VP micelles incorporating fluorescent dyes in water, 25 mg of PS-b-P4VP block copolymer and fluorescent dyes were first dissolved in 2 mL of N,N-dimethylformamide (DMF). Then, the mixture of the polymer, dye, and DMF was added into 25 mL of water (pH 3.0), gently stirred using a syringe pump (infusion speed of 5 μL/min, Picoplus, Harvard Apparatus), resulting in spherical micelles composed of a

hydrophobic PS core and a protonated P4VP corona shell. Similarly, PS-b-PAA block copolymer (25 mg) and fluorescent dye in 2 mL DMF were dissolved in 25 mL of water at a pH of 9.0 for the preparation of anionic PS-b-PAA BCMs integrating dyes. These charged BCMs were then purified by dialysis until no fluorescence was detectable in the buffer solution. The hydrodynamic radius of the spherical BCMs was observed by an Electrophoretic Laser Scattering Spectrophotometer (ELS-8000, OTSUKA ELECTRONICS) and the spherical morphology of the BCMs was observed by a field-emission scanning electron microscope (FE-SEM, JEOL 7401F).

Microfluidic manipulations for the generation of alternating BCM droplets and introduction of release solvents

We controlled the volumetric flow rate through each inlet channel using a syringe pump. The BCMs and oleic acid (Sigma Aldrich) used as a continuous phase in the present study were pumped using 500 mL (1700 series, needle type) and 2.5 mL (1000 series, needle type) Hamilton Gastight syringes, respectively. The syringes were connected to the microfluidic channel with Tygon Teflon tubing (30 gauge). Syringe pumps from Harvard Apparatus (PHD 22/2000 Infusion/withdraw pumps and Picoplus) were employed in the infusion mode to introduce both aqueous solutions and an oil continuous phase into the channel inlets.

Distilled water (pH 9.0) used as a release solvent in the present study was pumped using 500 mL (1700 series, Needle type) Hamilton Gastight syringes.

Aqueous BCM droplets generated from the inlet channels were observed at 8,000 fps by a high-speed video camera (FASTCAM ultim 512, Photron, Japan).

Measurement of the fluorescence intensity of LbL multilayer films formed on the posts

The fluorescent micrographs of the LbL films deposited on the posts were taken using an Olympus IX71 optical microscope with wide-excitation green (11007v2), red (11007v0), and blue (11007v1) filter sets. The surface intensity plots were obtained from these fluorescent microscopic images using an image analysis program (Image Pro).

2.3. Results and Discussion

Oppositely charged BCMs were prepared by using block copolymers with the chemical structures shown in Figure 1A and 1D. The polystyrene (PS) segment can be the core block while poly(acrylic acid) (PAA) and poly(4-vinylpyridine) (P4VP) segments can be the corona block when these block copolymers are dissolved in good solvents only for corona blocks. As we previously demonstrated (35), the degree of ionization (DOI) of PAA and P4VP segments can be easily tuned by adjusting the pH of the aqueous solution (35, 37). That is, a specific pH range of $3.0 < pH < 5.5$ can allow the two different coronas, PAA and P4VP, to be oppositely charged and to be assembled into multilayer films with PS-b-PAA and PS-b-P4VP micelles. In the case of a solution $pH > 5.5$, PAA segments can be fully charged. However, the DOI of the P4VP segments can be negligible. Based on this previous result, when the pH of the aqueous solution is adjusted to 9.0, multilayer films including PS-b-PAA and PS-b-P4VP micelles can be destructed.

The spherical morphologies of the BCMs used in the present study are shown in Figure 1D and 1E and the average hydrodynamic diameters of the PS-b-P4VP BCMs dissolved in an aqueous solution at a pH of 3 and PS-b-PAA BCMs dissolved in an aqueous solution at a pH of 6 are about 70 and 25 nm, respectively, as shown in Figure 1C and 1F.

Based on this concept, we performed multilayer deposition using alternating droplets with a charged BCM pair, PS-b-PAA (pH 6) and PS-b-P4VP (pH 4), onto a patterned post fixed in a cross-shaped microfluidic channel (Figure 2A). We also evaluated the continuous degradation of BCM multilayer films deposited onto the post modulated by the pH and shear stress of the release solvents (Figure 2B).

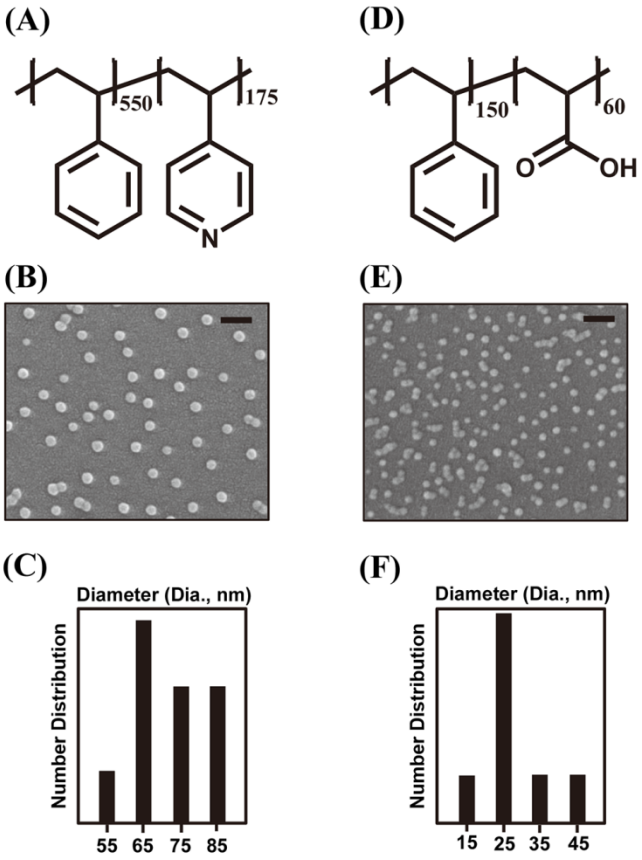

Figure 1. BCMs used for the LbL deposition and release in this study: (A-C) for PS-b-P4VP and (D-F) for PS-b-PAA. The chemical structures are shown in (A) and (D): field emission scanning electron microscopy (FE-SEM) images of BCMs in aqueous solution (1 mg / mL) @ pH 4 and pH 6 are shown in (B) and (E) (All scale bars shown the figures are 100 μm): hydrodynamic diameter distributions of BCMs measured by a electrophoretic laser scattering spectrophotometer (ELS) are shown in (C) and (F).

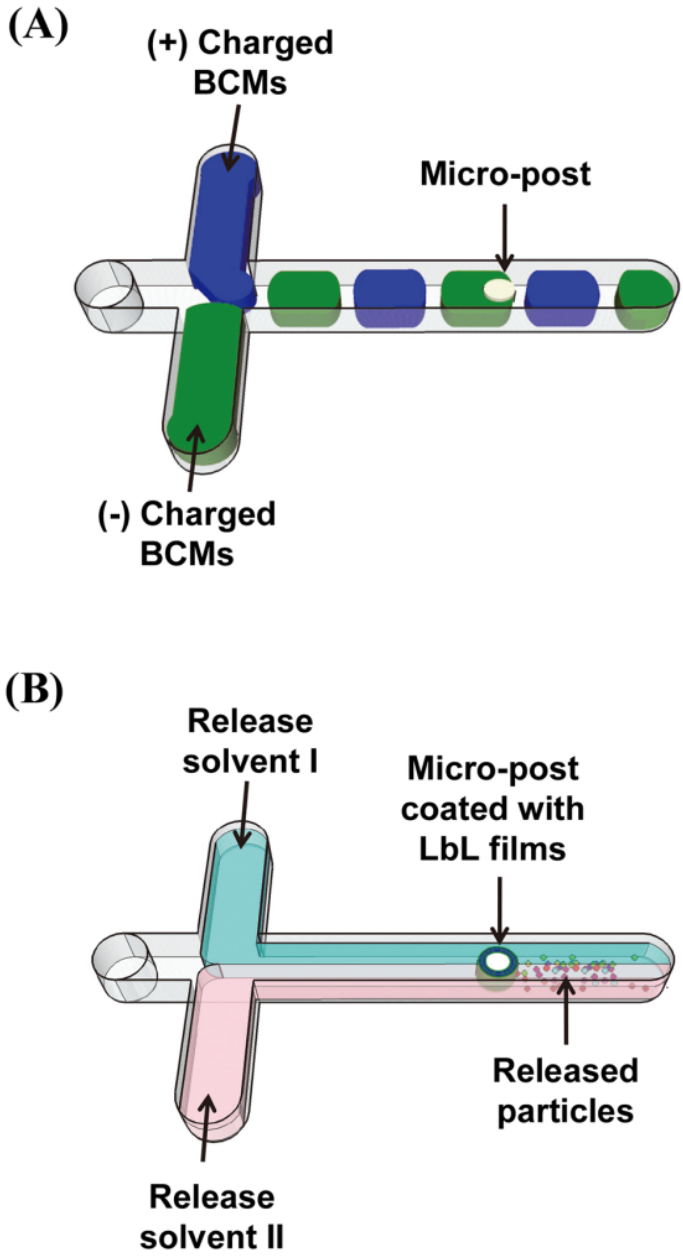

Figure 2. A schematic on the microfluidic device for LbL deposition (A) and for Janus degradation (B) of BCM multilayer films onto a patterned post

We utilized experimental flow conditions for alternating adsorption based on a previous study where the optimal range of the capillary number (Ca) of the continuous phase for successful alternating droplet generation (44) lies in the range of $0.001 < Ca < 0.051$ since the droplets generated in this regime form plugs, with a droplet diameter larger than the cross-sectional dimension of a microfluidic channel, capable of full contact with a patterned post. In the present study, Ca was fixed at 0.007 in all droplet-based LbL deposition experiments. The flow rate fraction (R_f) of the dispersed phase over the continuous phase was also fixed at the minimum value of 0.2, implying a maximum distance between neighboring droplets since the positively- and negatively-charged BCM droplets can easily aggregate together due to their attractive electrostatic interaction (45).

The patterned post, serving as a substrate for the BCM deposition, was generated using a photo-curable polymer, PEGDA (poly(ethylene glycol) diacrylate), in the microfluidic channel based on optofluidic maskless lithography46 where arbitrary shapes and sizes of microposts can be generated using this patterning method.

In Figure 3A, the BCM droplet flows around the patterned posts after the impact on a cone-shaped micro-post captured by a high speed camera are shown. In the case of this conical post, BCM droplets almost entirely contact the whole post including the back region. Based on the dynamics of droplets impacting a patterned post, we prepared PS-b-PAA BCMs incorporating FITC and PS-b-P4VP BCMs incorporating pyrene dyes to observe the distribution of adsorbed BCMs on a post. As shown in Figure 3B, the fluorescently labeled BCMs are uniformly adsorbed around the post including the back region. That is, two different fluorescent images emitted from the BCM multilayer films onto a single post were taken using filter sets for green or blue emission. In addition, the thickness of the BCM

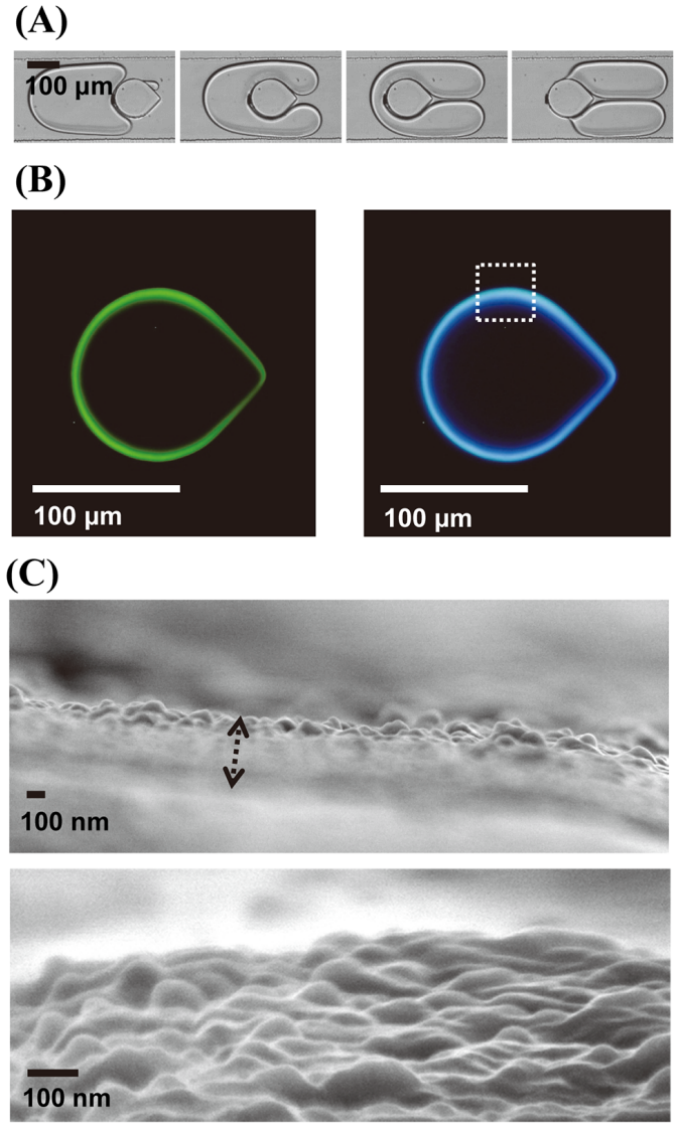

Figure 3. (A) BCM droplet motions, captured by a high speed camera, around a patterned post; (B) plan-view fluorescent images taken with filter sets only for green or blue emission and their surface intensity plot of BCMs deposited onto a single patterned post using a pair of PS-*b*-P4VP micelles incorporating Pyrene dyes and PS-*b*-PAA micelles incorporating FITC dyes; (C) top-view (left) and tilted (right) FE-SEM images of BCM multilayer films as depicted in figure 3(B).

multilayer films depicted in Figure 3B is approximately 300-400 nm, as shown in the top-view FE-SEM image in Figure 3C. We also observed nanometer scale lumpy topology of the BCMs in the tilted FE-SEM images. That is, for the same process time, 150 min in this case, conventional dip LbL, which usually takes approximately 40 min per bilayer formation, yielded a much lower thickness (~4 bilayers with a thickness of ~20 nm (35)) in comparison to the film thickness of about 300 nm achieved in the current droplet-based LbL deposition method. In addition, the amount of BCM solution consumed for the deposition of a ~300 nm thick BCM film was about 150 μL in the microfluidic device (i.e., 0.5 μL min-1 for 150 min with two kinds of BCMs), which is much less than the volume required for the dip LbL (~20 mL/bilayer required) to achieve the same BCM film thickness on a substrate.

In order to confirm the effect of the solution pH as well as shear rate on the degradation of BCM films deposited onto the post, we converted the experimental system from two-phase flow (droplet system) to one-phase flow (laminar flow system).

As observed by Lvov et al. (47), the laminar flow system was utilized for the formation of anisotropic micropatterns using electrostatic interactions between PE streams and spherical substrates. In one inlet channel, a PE solution was introduced, while the other inlet channels were filled with distilled water to realize selective deposition of PE molecules on half of the spherical microparticles fixed in the center of the microreactor channel. However, in these deposition systems driven by electrostatic interactions, although PE molecules are continuously provided, the adsorbed amount of PEs is limited until reversal of the surface charge, unless other PE streams with opposite charges are introduced.

In the present study, we first suggest a laminar flow system in which it is possible to degrade the multilayer film deposited on microposts by providing a continuous and pristine release

fluid. To precisely demonstrate the effect of solution pH on the destruction of the BCM multilayer films, two different streams were simultaneously introduced: a basic aqueous solution (pH 9), which allows combining the effects of adjusting the solution pH as well as shear rate, in addition to oleic acid modulated by only the shear rate. Moreover, the volumetric ratio between the two streams can control the spatial contact area with the micropost resulting in varying degradation regions of the BCM multilayer films. In the present experiment, the volumetric ratio of the aqueous solution was fixed at 0.3. Based on this condition, we experimentally investigated the in situ degradation behavior of the BCM films deposited on a single post as a function of the contact time with release solvents, as inferred from the decreasing fluorescent intensity of the dyes incorporated into the BCMs.

As shown in Figure 4A, the BCM multilayer films deposited onto a cylindrical post were assembled using oppositely charged PS-b-P4VP BCMs incorporating Nile red dyes and PS-b-PAA BCMs under the same experimental conditions as those in Figure 3. To compare the effect on the degradation of the red fluorescent BCM multilayer films, two different flows, a basic aqueous solution and oleic acid, were introduced in this channel, as shown in Figure 4B. The red fluorescent intensity of the area of the BCM multilayer films touched with the basic aqueous solvent was gradually decreased as the reaction time increased and the intensity of the area was finally negligible after 160 min. However, the fluorescent intensity of the area of the BCMs touched with the oleic acid medium was slightly decreased (Figure 4C-4F)). That is, multilayer films tightened with electrostatic attractions could be fully destructed by elimination of the attractive interaction during a similar modulation time as that employed for the multilayer deposition.

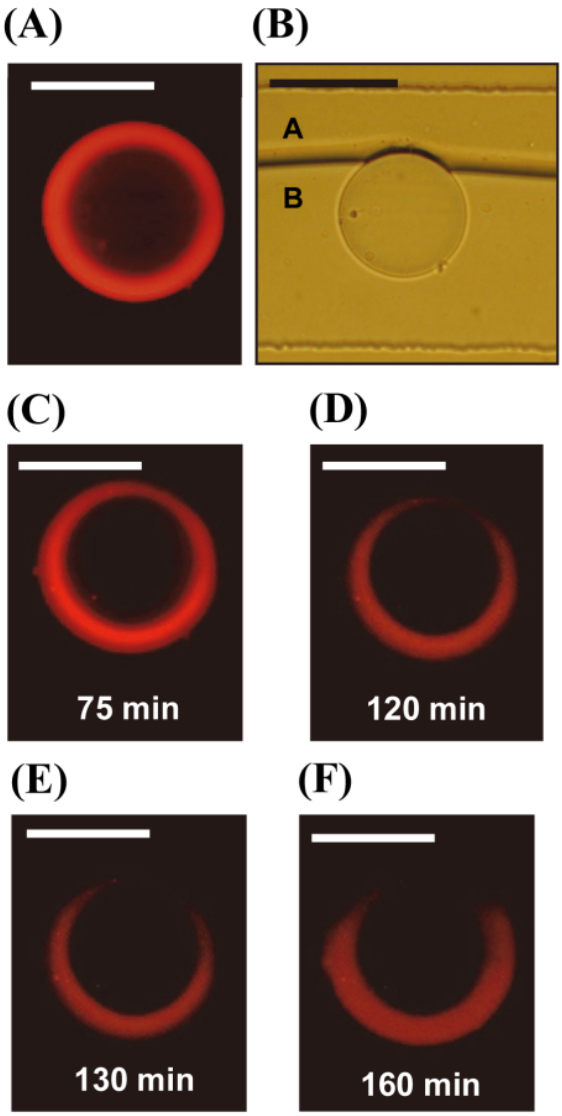

Figure 4. (A) A fluorescent image and (B) optical image of BCMs deposited using a pair of PS-b-P4VP micelles incorporating Nile red dyes and PS-b-PAA micelles for 150 min (capital A and capital B indicate basic aqueous solution and oleic acid, respectively); (C-F) fluorescent images taken at different release time (75, 120, 130, 160 min). (All scale bars shown in the figures are 100 μm.)

We also investigated the Janus destruction of BCM multilayer films deposited onto dual posts. In our previous works26, 48, the minimum distance between the centers of two posts to induce the droplet-based LbL deposition of linear polyelectrolytes on a single post was experimentally and numerically confirmed to be equivalent to the channel width (200 μm) in the same experimental environment employed currently. This suggests that an incoming fluid would be able to penetrate deep enough into the centerline between the two posts over the 200 μm center-to-center distance.

Based on the previous studies, we prepared two cylindrical posts with a center-to-center distance of 500 μm oriented in the flow direction, as depicted in Figure 5. We allowed droplets with oppositely charged PS-b-P4VP BCMs incorporating Nile red dyes and PS-b-PAA BCMs to pass around the dual posts and obtained fluorescent microscopy images of the red fluorescent-probed BCMs adsorbed onto both posts, as shown in Figure 5A. The degradation of the BCMs deposited onto the two posts was also observed as functions of the contact times with basic aqueous solvents (pH 9) and oleic acid, as shown in Figure 5B and C, respectively, where the trends are similar to those of the single post system shown in Figure 4. The red fluorescent intensity of the area of the BCM multilayer films contacting the basic aqueous solvent gradually decreased as the reaction time increased, where the intensity of the area was finally negligible after 160 min. However, the fluorescent intensity of the area of the BCMs contacting oleic acid was slightly decreased. That is, the minimum distance between two neighboring posts for the Janus BCM multilayer films decorated onto microposts is the same as the minimum distance for the droplet-based LbL deposition since the distance for those laminar flows is sufficient to behave like the droplet flow around an isolated post.

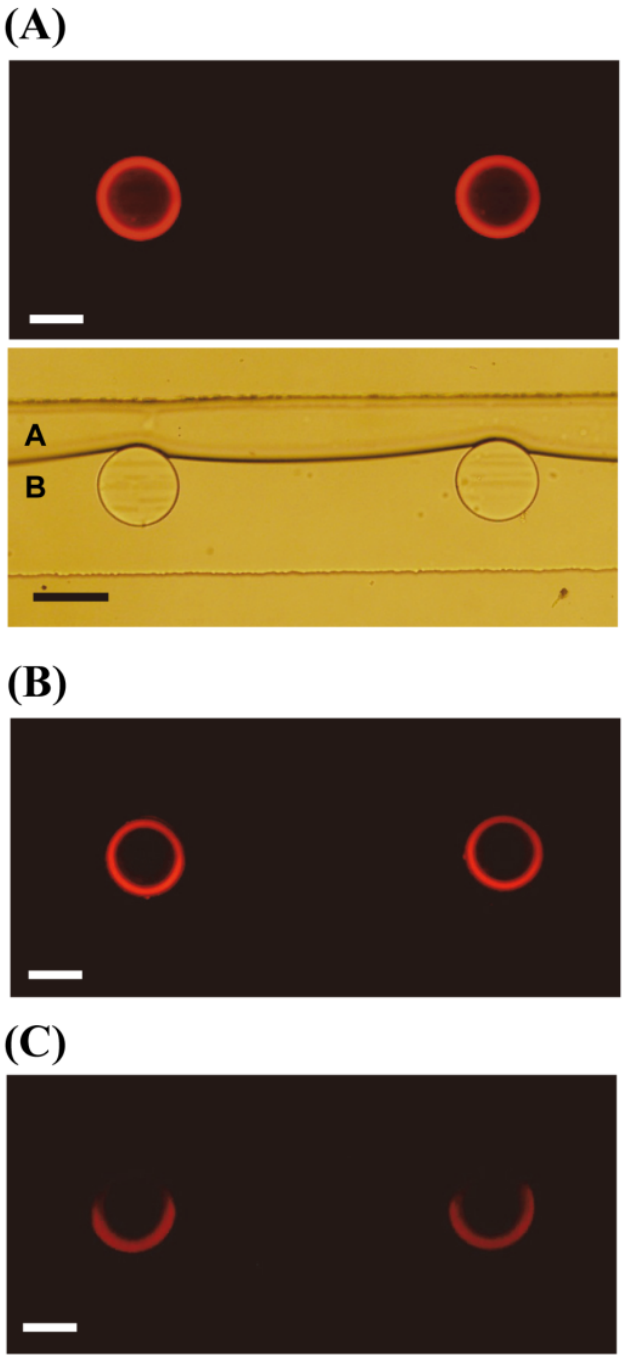

Figure 5. (A) A fluorescent image and optical image of BCMs deposited onto dual posts using a pair of PS-b-P4VP micelles incorporating Nile red dyes and PS-b-PAA micelles for 150 min (capital A and B indicate basic aqueous solution and oleic acid, respectively); (B, C) fluorescent images taken at different release time (60, 160 min) (All scale bars shown in the figures are 100 μm.).

It is interesting to note that all of the fluorescent microscopic images shown in Figure 4 and 5 were obtained while the contrast and brightness were fixed, respectively. This implies that the deposition as well as destruction of the BCM multilayer films were attained in a single microfluidic channel at the identical modulation time (150 min) and flow rate (2 μL/min) because the driving forces for both deposition and degradation, the electrostatic interactions and shear rate, were identical. Therefore, from the perspective of adsorption kinetics, the microfluidic technique introduced here can provide a tool to study the two driving forces of shear rate and electrostatic interaction at the same time, which is a not possible using earlier experimental technique.

2.4. Conclusion

A simple cross-shaped microfluidic channel was employed for the preparation of alternating aqueous droplets containing oppositely charged block copolymer micelles (BCMs). The BCM droplets alternately impacted the patterned posts to induce the deposition of the oppositely charged BCMs (a pair of PS-b-PAA BCMs @ pH 6 and PS-b-P4VP BCMs @ pH 4) in a specific range of the capillary number (Ca) of the continuous phase, resulting in BCM multilayer films with thicknesses of hundreds of nanometers with a small amount of BCM solutions in a short process time. In addition, the cross-shaped microfluidic channels with BCMs deposited onto posts was utilized for the visualization of selective and continuous destruction of BCM multilayer films using two different laminar streams, basic distilled water as a release solvent (pH 9) and oleic acid as a non-reactive medium, since the degree of ionization of P4VP segments is negligible above a pH of 5.5. That is, BCM multilayer films deposited for 150 min with a thickness of 300 nm were selectively removed from the posts, being contacted with the aqueous release solvent with a pH of 9, until an exposure time of 160 min, which is similar to the deposition time. However, the decrease of the fluorescent intensity on the BCM films contacting the stream of the non-reactive medium, to induce destruction only by the shear rate, was negligible after an exposure time of 160 min. Therefore, in the present work, we demonstrated both the deposition as well as destruction of BCM multilayer films in a single microfludic channel by identical driving forces, electrostatic interaction and shear rate, at an identical modulation time and flow rate.

2.5. References

1. R. Duncan, The dawning era of polymer therapeutics. Nat. Rev. Drug Discov. 2, 347 (May, 2003).
2. K. L. Kiick, Polymer Therapeutics. Science 317, 1182 (August 31, 2007, 2007).
3. A. V. Kabanov, P. L. Felgner, L. W. Seymour, Self-assembling Complexes for Gene Delivery. From Laboratory to Clinical Trial.Self-assembling Complexes for Gene Delivery.From Laboratory to Clinical Trial (Wiley, 1998).
4. L. G. Donaruma, Synthetic biologically active polymers. Progr.Polym.Sci. 4, 1 (1974).
5. R. Duncan, S. Dimitrijevic, E. G. Evagorou, The role of polymer conjugates in the diagnosis and treatment of cancer. S. T. P. Pharma Sciences 6, 237 (1996).
6. R. Langer, D. A. Tirrell, Designing materials for biology and medicine.Nature 428, 487 (2004).
7. M. P. Lutolf, J. A. Hubbell, Synthetic biomaterials as instructive extracellular microenvironments for morphogenesis in tissue engineering. Nat. Biotechnol. 23, 47 (2005).
8. C. Fischbach, D. J. Mooney, Polymers for pro- and anti-angiogenic therapy.Biomaterials 28, 2069 (2007).
9. B. S. Kim, S. W. Park, P. T. Hammond, Hydrogen-bonding layer-by-layer assembled biodegradable polymeric micelles as drug delivery vehicles from surfaces. ACS Nano 2, 386 (Feb, 2008).
10. B. Qi, X. Tong, Y. Zhao, Layer-by-Layer Assembly of Two Different Polymer Micelles with Polycation and Polyanion Coronas. Macromolecules 39, 5714 (2006).
11. D. Volodkin et al., Composite multilayered biocompatible polyelectrolyte films with

intact liposomes: stability and temperature triggered dye release. Soft Matter 4, 122 (2008).

12. P. T. Hammond, Thin films: Particles release. Nat. Mater. 9, 292 (2010).

13. Y. Lvov, K. Ariga, I. Ichinose, T. Kunitake, Assembly of Multicomponent Protein Films by Means of Electrostatic Layer-by-Layer Adsorption. J. Am. Chem. Soc. 117, 6117 (1995/06/01, 1995).

14. F. Caruso, R. A. Caruso, H. Möhwald, Nanoengineering of Inorganic and Hybrid Hollow Spheres by Colloidal Templating.Science 282, 1111 (November 6, 1998, 1998).

15. J. Hiller, J. D. Mendelsohn, M. F. Rubner, Reversibly erasable nanoporous anti-reflection coatings from polyelectrolyte multilayers. Nat. Mater. 1, 59 (2002).

16. P. Podsiadlo et al., Ultrastrong and stiff layered polymer nanocomposites. Science 318, 80 (Oct 5, 2007).

17. J. Hong, K. Char, B.-S. Kim, Hollow Capsules of Reduced Graphene Oxide Nanosheets Assembled on a Sacrificial Colloidal Particle. J. Phys. Chem. Lett. 1, 3442 (2010).

18. S. W. Lee et al., High-power lithium batteries from functionalized carbon-nanotube electrodes. Nat. Nanotechnol. 5, 531 (Jul, 2010).

19. Y. Kim, C. Lee, I. Shim, D. Wang, J. Cho, Nucleophilic Substitution Reaction Based Layer-by-Layer Growth of SuperparamagneticNanocomposite Films with High Nonvolatile Memory Performance. Adv. Mater. 22, 5140 (2010).

20. W. K. Bae et al., Multicolored Light-Emitting Diodes Based on All-Quantum-Dot Multilayer Films Using Layer-by-Layer Assembly Method. Nano Lett. 10, 2368 (2010/07/14, 2010).

21. G. Decher, Fuzzy Nanoassemblies: Toward Layered Polymeric Multicomposites. Science 277, 1232 (August 29, 1997, 1997).

22. J. Cho, K. Char, J. D. Hong, K. B. Lee, Fabrication of Highly Ordered Multilayer Films Using a Spin Self-Assembly Method. Adv. Mater. 13, 1076 (2001).

23. P. A. Chiarelli et al., Controlled Fabrication of Polyelectrolyte Multilayer Thin Films Using Spin-Assembly. Adv. Mater. 13, 1167 (2001).

24. C. H. Porcel et al., Ultrathin Coatings and (Poly(glutamic acid)/Polyallylamine) Films Deposited by Continuous and Simultaneous Spraying. Langmuir 21, 800 (2005/01/01, 2004).

25. J. B. Schlenoff, S. T. Dubas, T. Farhat, Sprayed Polyelectrolyte Multilayers. Langmuir 16, 9968 (2000).

26. M. Lee et al., Multilayer deposition on patterned posts using alternating polyelectrolyte droplets in a microfluidic device. Lab Chip 10, 1160 (2010).

27. C. Priest et al., Microfluidic polymer multilayer adsorption on liquid crystal droplets for microcapsule synthesis. Lab Chip 8, 2182 (2008).

28. H.-J. Kim, K. Lee, S. Kumar, J. Kim, Dynamic Sequential Layer-by-Layer Deposition Method for Fast and Region-Selective Multilayer Thin Film Fabrication.Langmuir 21, 8532 (2005).

29. K. Kataoka, A. Harada, Y. Nagasaki, Block copolymer micelles for drug delivery: design, characterization and biological significance. Advanced Drug Delivery Reviews 47, 113 (Mar 23, 2001).

30. J. Kreuter, Nanoparticles, in colloidal drug delivery systems. M. Dekker, Ed., Nanoparticles, in colloidal drug delivery systems (New York 1994).

31. P. D. Scholes, A. G. A. Coombes, M. C. Davis, L. Illum, S. S. Davis, Particle

engineering of biodegradable colloids for site-specific drug delivery. C. D. Delivery, Ed., Particle engineering of biodegradable colloids for site-specific drug delivery (American Chemical Society, 1997).

32. G. S. Kwon, T. Okano, Polymeric micelles as new drug carriers. Advanced Drug Delivery Reviews 21, 107 (1996).

33. K. Emoto, M. Iijima, Y. Nagasaki, K. Kataoka, Functionality of Polymeric Micelle Hydrogels with Organized Three-Dimensional Architecture on Surfaces. J. Am. Chem. Soc. 122, 2653 (2000).

34. N. Ma, H. Zhang, B. Song, Z. Wang, X. Zhang, Polymer Micelles as Building Blocks for Layer-by-Layer Assembly: An Approach for Incorporation and Controlled Release of Water-Insoluble Dyes. Chem. Mat. 17, 5065 (2005).

35. J. Cho, J. Hong, K. Char, F. Caruso, Nanoporous Block Copolymer Micelle/Micelle Multilayer Films with Dual Optical Properties. J. Am. Chem. Soc. 128, 9935 (2006).

36. J. Seo, J. L. Lutkenhaus, J. Kim, P. T. Hammond, K. Char, Development of Surface Morphology in Multilayered Films Prepared by Layer-by-Layer Deposition Using Poly(acrylic acid) and Hydrophobically Modified Poly(ethylene oxide). Macromolecules 40, 4028 (2007/05/01, 2007).

37. J. Hong et al., Tunable superhydrophobic and optical properties of colloidal films coated with mock copolymer micelles/micelle multilayers. Adv. Mater. 19, 4364 (Dec 17, 2007).

38. E. Donath, G. B. Sukhorukov, F. Caruso, S. A. Davis, H. Mohwald, Novel hollow polymer shells by colloid-templated assembly of polyelectrolytes. Angew.Chem.-Int. Edit. 37, 2202 (Aug 17, 1998).

39. J. El-Ali, P. K. Sorger, K. F. Jensen, Cells on chips. Nature 442, 403 (07/27/print,

2006).

40. I. Meyvantsson, D. Beebe, Cell culture models in microfluidic systems. Annual Review of Analytical Chemistry, (2008), vol. 1, pp. 423-449.

41. J. H. Sung et al., Microfabricated mammalian organ systems and their integration into models of whole animals and humans. Lab Chip 13, 1201 (2013).

42. H. A. Stone, Dynamics of Drop Deformation and Breakup in Viscous Fluids. Annu Rev Fluid Mech 26, 65 (1994).

43. L. H. Hung et al., Alternating droplet generation and controlled dynamic droplet fusion in microfluidic device for CdS nanoparticle synthesis. Lab Chip 6, 174 (Feb, 2006).

44. S. E. Chung et al., Optofluidicmaskless lithography system for real-time synthesis of photopolymerized microstructures in microfluidic channels. Appl. Phys. Lett. 91, 041106 (2007).

45. D. G. Shchukin et al., Polyelectrolyte Micropatterning Using a Laminar-Flow Microfluidic Device. Adv. Mater. 16, 389 (2004).

46. C. Chung, M. Lee, K. Char, K. H. Ahn, S. J. Lee, Droplet dynamics passing through obstructions in confined microchannel flow. Microfluid.Nanofluid.9, 1151 (2010).

47. J. C. McDonald et al., Fabrication of microfluidic systems in poly(dimethylsiloxane). Electrophoresis 21, 27 (Jan, 2000).

48. J. C. McDonald, G. M. Whitesides, Poly(dimethylsiloxane) as a Material for Fabricating Microfluidic Devices. Acc. Chem. Res. 35, 491 (2002/07/01, 2002).

CHAPTER III

Inter-Corona Complexation Induced by Subsequent Mixing of Oppositely Charged Block Copolymer Micelles

3.1. Introduction to Polyelectrolyte Complexes

In general, mixing solutions of a polyanion and a polycation leads to spontaneous aggregation with the release of the counterions, polyelectrolyte complexes (PECs) (1-23). In the early 1930's, Bungenberg de Jong et al found that mixing aqueous solutions of oppositely charged natural polyelectrolytes (e.g. gelatin and gum arabic), under certain conditions, a phase separation and formation of liquid coacervates took place (3,4).

One of soft colloids, block copolymer micelle (BCM) has been intensively studied because polymeric micelle composition and shape can be simply designed through monomer selection, chain architecture design, and variation of solution conditions (e.g., solvent mixtures, pH manipulation, salt concentration and temperature) (24-30).

From now on, many researchers have reported about polyelectrolyte (PE) complexes using poly(acrylic acid) (PAA) and poly(4-vinyl pyridine) (P4VP) as a model system since they can be interacted with hydrogen bonding or electrostatic interaction in solution. As Eisenberg and coworkers reported, mixture of PS-b-PAA and PS-b-P4VP block copolymers can be self-assembled into various morphologies in aqueous media by varying block length ratios between PAA and P4VP or solution condition such as initial pH. However, it is difficult to demonstrate PAA and P4VP complexation in a whole range of pH using this conventional

experimental protocol since they can be oppositely charged in specific pH region resulting in aggregation or precipitation.

Therefore, we suggest subsequent mixing of BCMs to be interacted between oppositely charged coronas as a new assembling pathway. This mixing protocol can provide both of the corona-corona complexation and the interfacial rearrangement. Those complex morphologies of polymeric nanoparticles assembled in the present system can be obtained from their structural flexibility which would not be accessible in earlier experimental conditions using hard spheres.

3.2. Experimental Section

Preparation of individual BCMs

PS-b-P4VP (polystyrene-block-poly(4-vinylpyridine), Mw(PS) = 57,500, Mw(P4VP) = 18,500, PDI = 1.15) and PS-b-PAA (polystyrene-block-poly(acrylic acid), Mw(PS) = 15,000, Mw(PAA) = 4,300, PDI = 1.15) were purchased from Polymer Source. For the preparation of protonated PS-b-P4VP micelles incorporating fluorescent dyes in water, 25 mg of PS-b-P4VP block copolymer and fluorescent dyes were first dissolved in 2 mL of N,N-dimethylformamide (DMF). Then, the mixture of the polymer, dye, and DMF was added into 25 mL of water (pH 3.0), gently stirred using a syringe pump (infusion speed of 5 μL/min, Picoplus, Harvard Apparatus), resulting in spherical micelles composed of a hydrophobic PS core and a protonated P4VP corona shell. Similarly, PS-b-PAA block copolymer (25 mg) and fluorescent dye in 2 mL DMF were dissolved in 25 mL of water at a pH of 9.0 for the preparation of anionic PS-b-PAA BCMs. These charged BCMs were then purified by dialysis until no fluorescence was detectable in the buffer solution. The hydrodynamic radius of the spherical BCMs was observed by an Electrophoretic Laser Scattering Spectrophotometer (ELS-8000, OTSUKA ELECTRONICS) and the spherical morphology of the BCMs was observed by a field-emission scanning electron microscope (FE-SEM, JEOL 7401F).

Subsequent mixing of BCMs

The ratio of PAA from PS-b-PAA to P4VP from PS-b-P4VP blocks was fixed as 1:1. The total polymer concentration was fixed to 1 %.

3.3. Results and Discussion

Materials used in the present study are PS-b-P4VP BCMs as cationic nanoparticles (NPs) and PS-b-PAA BCMs, carboxylated polystyrene particles (PS-COOH), carboxylated quantum dots (QD-COOH), and PAA homopolymers as anionic NPs as shown in Table 1.

Effect of solution pH

In previous study of our group (31-33), PS-b-PAA and PS-b-P4VP BCMs was first introduced as nanometer scale carriers for functional multilayer films. The charge densities of the corona blocks (either PAA or P4VP blocks) dispersed in water were quite sensitive to solution pH. In general, the morphology of BCMs can be determined by intra-molecular repulsion within a micelle (34, 35). Therefore, morphology of BCM complexes induced by combination of those PAA or P4VP coronas can be also varied by solution pH.

To determine the effective pH range for the inter-corona combination of PAA and P4VP dissolved together in aqueous media, we studied interaction forces between two coronas using Fourier Transfer Infrared Spectroscopy (FT-IR) as shown in Fig. 1(a) (36). It shows that dominant binding mechanism between PAA and P4VP is electrostatic interaction (1640 ~ 1650, 1500 cm^{-1}) as well as hydrogen bonding force (1400 ~ 1450) at pH 4 (37, 38). When the solution pH decreases up to 1.0, uncharged carboxylic acid (-COOH) absorption band at about 1700 cm-1 appears. In addition, charged carboxylic acid (-COO-) absorption band seen at solution pH 14.0 has much higher peak intensity than that of peak seen at 1640 cm^{-1}. Although mixing ratio of repeat units of two homopolymers is identical, degree of actual

Cationic NPs (Mw, Diameter)			Anionic NPs (Mw, Diameter)	
Poly(styrene)-*block*-Poly(4-vinylpyridine), PS-*b*-P4VP 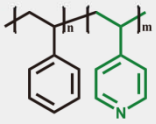	163-*b*-466 	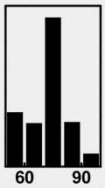	Poly(styrene)-block-Poly(acrylic acid), PS-*b*-PAA 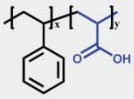	144-*b*-60 (~ 20 nm) 
	552-*b*-176 		Carboxylated PS Latex Particles, PS-COOH	~ 20 nm 
	260-*b*-162 	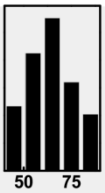	Carboxylated Quantum Dots, QD-COOH	~ 7 nm 
	230-*b*-18 	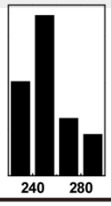	Poly(acrylic acid), PAA Homopolymers 	28 

Table 1.Materials used in the present study. The compositions of blocks are indicated by x-b-y, where x is the number of styrene units and y is the number of 4-vinylprydine or acrylic acid units in the chain. The hydrodynamic diameter of these nanoparticles (NPs) was measured by a electrophoretic laser scattering spectrophotometer (ELS).

complexation can be controlled by solution pH. That is, when the two blocks, P4VP and PAA,are stoichiometrically mixed in an aqueous solution, one of those blocks can be preferentially ionized, PAA at pH 14, P4VP at pH 1. However, they can be entirely interacted each other at pH 4.

Each of PS_{144}-PAA_{60} BCMs and PS_{552}-$P4VP_{176}$ BCMs morphologies were spherical as shown in Fig. 1(b). Their complex Morphology mixed at pH 4 was shown in Fig. 1(c)-(e) as a function of stirring time. When they are mixed together for 12 hrs, they formed bigger spherical BCMs and hexagonal rod-like BCMs. The diameter as well as length of the rod was getting bigger and they are formed hexagonal prism-like structures of hundreds of nanometer scale.

To understand this complexation, morphologies of individual BCMs at various solution pH were needed to be examined. In a pH region of $3.5 < pH < 5.0$, PS_{552}-b-$P4VP_{176}$ and PS_{144}-b-PAA_{60} block copolymers were self-assembled into spherical BCMs with hydrodynamic diameters of about 75 nm and 25 nm, respectively. However, in the higher pH region ($5.5 < pH < 9$), PS_{552}-b-$P4VP_{176}$ block copolymers were transformed into large compound micelles (LCMs) with hydrodynamic diameters over 300 nm. In general, the ionization of P4VP blocks is negligible at $pH > 5.5$ so that solubility in water sharply decreased. The PS_{144}-b-PAA_{60} BCMs were remained their morphology and their size is slightly enlarged due to repulsion among their fully charged coronas. In a same manner, in a lower pH region ($pH < 2.0$), the PS_{144}-b-PAA_{60} was formed to LCMs with hydrodynamic diameter of 200 nm due to corona's ionization decrease and PS_{552}-b-$P4VP_{176}$ BCMs is a little enlarged due to repulsion among their fully charged P4VP segments.

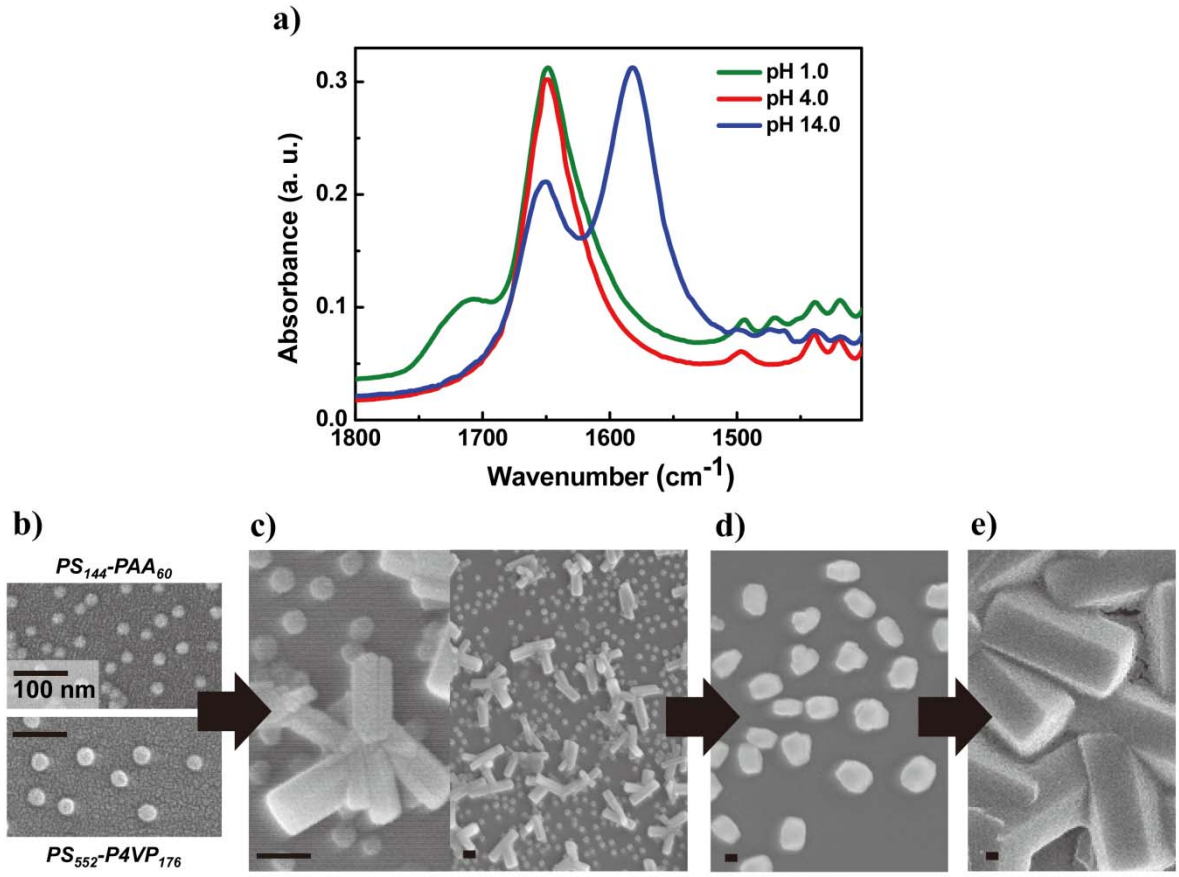

Fig. 1 (a) Investigation of interaction between PAA and P4VP homopolymers at various solution pH by Fourier Transfer Infrared Spectroscopy (FT-IR); (b) Each PS-b-PAA & PS-b-P4VP BCMs were observed by a field-emission scanning electron microscope (FE-SEM) images in prior to mixing together; (c)-(e) FE-SEM images of BCM complexes as a function of stirring time, 12 hrs, 2 days, and 5 days.

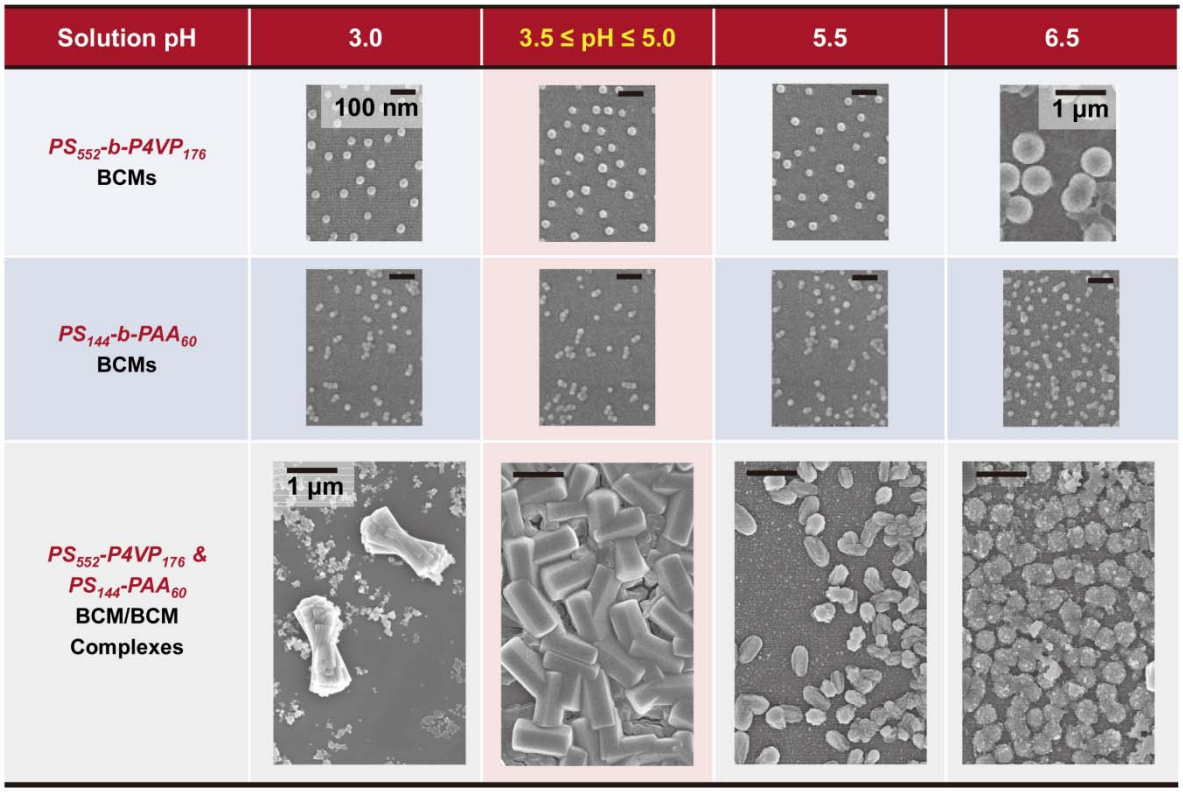

Fig. 2 Morphology of BCM complexes by varying solution pH

Based on the FT-IR result and morphology of individual BCMs, complex morphology of PS-b-P4VP BCMs and PS-b-PAA BCMs was investigated using FE-SEM at various solution pH as represented in Fig. 2. The complex morphology of the BCMs in a range of $3.5 < pH < 5.0$ was observed to hexagonal prism-like structures. When the solution pH increases to 6.5, these two BCMs are self-assembled into hierarchical bumpy spheres induced by mere mixing of small PS-b-PAA BCMs and PS-b-P4VP LCMs. In addition, those morphologies are reversibly obtained by switching solution pH from 3.0 to 6.5 or vice versa. That is, if corona-corona interaction is relatively strong within effective pH region, combination of oppositely charged BCMs provides inter-corona complexation as well as rearrangement of interfacial curvature resulting in hexagonal prism structures. However, if corona-corona interaction is relatively weak within effective pH region, only inter-corona complexation occurs.

When the solution pH increases over the effective pH range or decreases below the effectivepH range, surface charge of BCM complexes was measured to fully negative or positive value unlike neutral surface at the effective pH region. That is, when the solution pH is changed beyond the effective solution pH region for BCM & BCM complexation, one of the two coronas is preferentially segregated into coronas.

Combination effect of Mw ratio & DMF content

In general, name of crew-cut suggests that length of the corona-forming block is very short compared to that of the core-forming block (39, 40). In order to reconfirm the pH-tunable morphologies of the crew-cut BCM complexes, we prepared PS_{230}-b-$P4VP_{18}$ / PS_{144}-b-PAA_{60} BCMs. As shown in Fig. 3 (b), the crew-cut BCM complex morphology was not hexagonal crystals but hierarchical bumpy spheres even though the pH of the aqueous solvent lies in

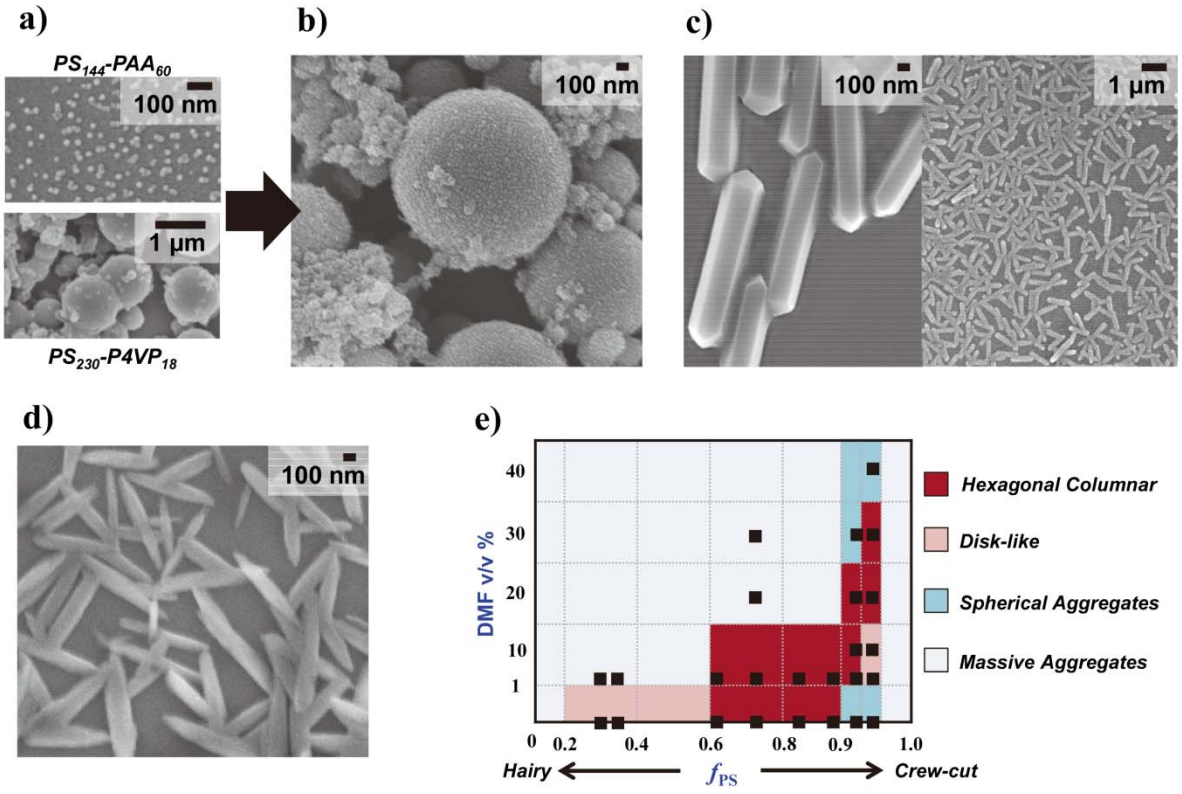

Fig. 3. Morphology of complexes with crew-cut or hairy PS-*b*-P4VP BCMs: (a) each morphologies of crew-cut PS-b-P4VP and PS-b-PAA BCMs; (b) & (c) complexes with crew-cut PS-b-P4VP BCMs dissolved in solvent mixture involving various DMF content, 0 % and 1 %; (d)) complexes with hairy PS-b-P4VP BCMs dissolved in solvent mixture involving DMF content, 0 %; (e) phase diagram of BCM complex morphology as a function of PS fraction and DMF content.

proper pH region (3.5 < pH < 5.0). These bumpy structures were induced by mere adsorption of small PS-b-PAA BCMs onto the surface of PS-b-P4VP LCMs with their original morphology remaining. That is, inter-corona complexation does not allow hexagonal prism structures without rearrangement of strongly aggregated core blocks. However, crew-cut BCM complexation in higher DMF content (1.0 % < DMF < 20 %) induces inter-corona combination resulting in hexagonal prism structures (fig. 3 (c)) because higher DMF ratio can lead to increase in solubility of all block segments.

In a same manner, name of hairy suggest that length of the core-forming block is very short compared to that of the corona-forming block (39, 40). To confirm the complex morphology including hairy micelles, PS_{230}-b-$P4VP_{542}$ / PS_{144}-b-PAA_{60} BCMs were prepared. As shown in Fig. 3 (d), the hairy BCM complex morphology was not hexagonal crystals but disk-like structures even though the pH of the aqueous solvent lies in proper pH region (3.5 < pH < 5.0). In addition, those complexes were changed their morphologies to massive aggregates in solution with higher DMF content.

To summarize this complexation behavior, BCM complexes are induced by combination effect of polystyrene DP (degree of polymerization) ratio and DMF content. (Fig. 3(e)) That is, there are two steps for hexagonal complexation: The first step is neutralization of P4VP coronas with PAA coronas. This step can be varied by solution pH and mixing ratio of P4VP and PAA units. The next step is secondary aggregation of the neutralized BCMs into rod-like structures. Content of co-solvent can be important to induce the interfacial rearrangement.

To justify the effect of micelle structures, crew-cur or hairy, various fraction of PS segments (f_{PS}, 0.2 ~ 0.95) were scanned. The fraction value of PS segments is approaching to 0.9, the

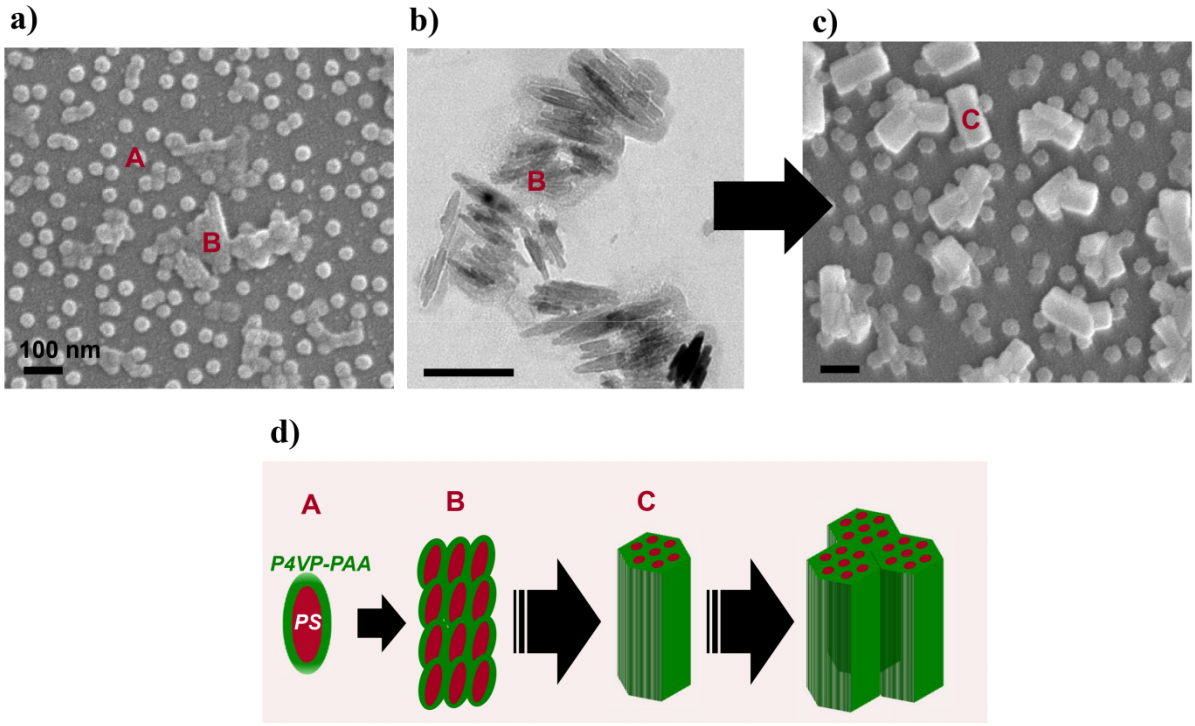

Fig. 4. FE-SEM & TEM images of BCM complexes in an early state (a)-(c) and possible mechanism of formation of hexagonal prism-like structures (d).

micelle structures can be named to crew-cut and the fraction of PS is approaching to 0.2, the micelle structures can be named to hairy. As shown in Fig. 3, the hexagonal prism structure can be obtained in the case of $f_{PS} > 0.6$ and at a specific DMF content. In addition, the DMF content to be needed to form the hexagonal prism structures is getting higher when the f_{PS} is approaching to 0.9.

Based on those results, we can suggest the mechanism for morphological transition from spherical BCMs to hexagonal prism-like structures. As shown in Fig 4, early state of BCM complexes can indicate assembly pathways. The spherical complexes with neutralized coronas (Fig. 4(a)) can be easily aggregated into rod-like structures with flatten interfaces between core and coronas (Fig. 4(b)). Those rod-like structures can be self-assembled into hexagonal prism structures (Fig. 4(c)) by long-range interactions between P4VP and PAA coronas.

Pochan&Wooley Group has used polystyrene-block-poly(acrylic acid) (PS-b-PAA) and divalent organic counter ions including long hydrophobic parts to drive the organization of the block copolymers into disk-like structures. In those complexes, repulsion between charged inter-coronas is screened by counter ions and the hydrophobic parts of diamine can be penetrated into PS core region. That is, interfacial curvature between core (PS) and corona (PAA) of the complexes was getting lower by reducing the inter-corona repulsion resulting in disk-like micelles with flatten interfaces between core and coronas (41).

Complexation of various counter ions (PAA homopolymers, QDs-COOH, PS Latexes-COOH)

To reconfirm this mechanism, various NPs was prepared PAA_{28}, QD-COOH (7 nm), and PS-

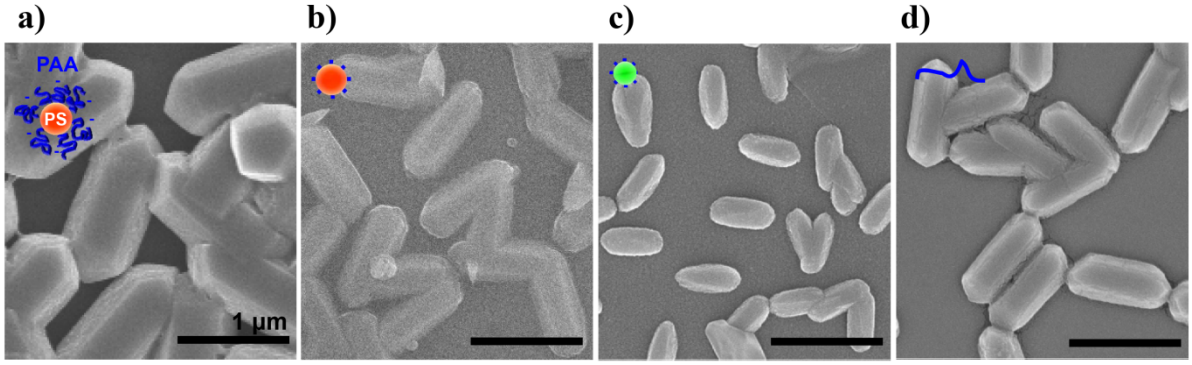

Fig. 5 (a)-(d) Complexes of PS_{552}-b-$P4VP_{162}$ BCMswith various anionic NPs such as PS_{144}-*b*-PAA_{60}, PS-COOH, QD-COOH, and PAA_{28}

COOH (20 nm) as a counter part of PS_{552}-b-$P4VP_{162}$ BCMs. As shown in Fig. 5, all morphologies of the BCM complexes are not spherical but hexagonal prism-like structures @ pH 4.

3.4. Conclusion

The morphology of charged BCM complexes, consisting of polystyrene-block-poly(acrylic acid) (PS-b-PAA) and polystyrene-block-poly(4-vinyl pyridine) (PS-b-P4VP) micelles, was controlled by pH of aqueous solvent as well as solvent quality. To determine the effective pH range for the inter-corona combination of PAA and P4VP blocks in aqueous media, we studied the dissociation behavior of both coronas using Fourier Transform Infrared Spectroscopy. Lower pH region ($3.6 < pH < 5.0$) in aqueous medium offers stronger interactions between oppositely charged corona blocks, resulting in polymeric hexagonal prism complexes. In the higher pH region ($5.5 < pH < 6.5$), they first self-assembled into hierarchical bumpy spheres induced by the simple adsorption of small PS-b-PAA BCMs on the surfaces of PS-b-P4VP large compound micelles since the degree of ionization of P4VP blocks is relatively low. However, the crew-cut BCM complex morphology with high aggregation number does not allow the hexagonal prism structure to be formed without rearranging strongly aggregated core blocks. We note that the crew-cut BCM complexation in higher DMF content of a mixed solvent (1 % < DMF < 20 % in water) induces inter-corona association leading to the hexagonal prism structure due to the decrease in selectivity of water for PS blocks.

1.1. References

1. Michaels, A. S.; Miekka, R. G. J. Phys. Chem. 1961, 65, 1765-1773.

2. Michaels, A. S. Ind. Eng. Chem. 1965, 57, 32-40.

3. Bungenberg de Jong, H. G. Trans. Faraday Soc., 1932, 28, 27.

4. Bungenberg de Jong, H. G.; Dekker, W. A. Kolloidchem. Beih., 1936, 43, 143.

5. Fuoss, R. M.; Sadek, H. Science 1949, 110, 552.

6. Dautzenberg, H. In Physical Chemistry of Polyelectrolytes; Radeva, T., Ed.; M.Dekker: New York, 2001; Chapter 20.

7. Kokufuta, E.; Matsumoto, W.; Nakamura, I. J. Appl. Polym. Sci. 1982, 27, 2503-2512.

8. Dautzenberg, H.;Lukanoff, B.; Eckert, U.; Tiersch, B.; Schuldt, U. Ber.Bunsenges. Phys. Chem. 1996, 100, 1045-1053.

9. Lysaght, M. J.; Aebischer, P. Scientific American 1999, 280, 76-82.

10. Dautzenberg, H.; Karibyants, N. Zaitsev, S. Y. Macromol. Rapid Commun. 1997,18, 175-182.

11. Anderson, M. A.; Hatti-Kaul, R.; J. Biotechnology 1999, 72, 21-31.

12. Kabanov, A. V.; Vinogradov, S. V.; Suzdaltseva, V. G.; Alakhov, V. Y. Bioconjugate. Chem. 1995, 6, 639-643.

13. Konak, C.; Mrkvickova, L.; Nazarova, O.; Ulbrich, K.; Seymour, L. W. Supramolecular Science 1998, 5, 67-74.

14. Wolfert, M. A.; Schacht, E. H.; Toncheva, V.; Ulbrich, K.; Nazarova, O.;Seymour, L. W. Human Gene Therapy 1996, 7, 21213-2133.146

15. Asayama, S.; Muruyama, A.; Cho, C. S.; Akaike, T. Bioconjugate. Chem. 1997,8, 833-838.

16. Kabanov, V. A. in Multilayer Thin Films. Sequential Assembly of Nanocomposite Materials Edited by Decher, G. and Schlenoff, J. B. Wiley-VCH, Weinheim, 2003. Chapter 2.

17. Kabanov, V. A.; Zezin, A. B.; Kasaikin, V. A.; Jaroslavov, A. A.; Topchiev, D.A.Usp. Khim. 1991, 160, 595-601.

18. Zezin, A. B.; Eltsefon, B. S.; Rudman, A. R.; Vengerova, N. A.; Kalyuzhnaya, R.I.; Valueva, S. P.; Kopilova, E. M.; Chepurov, A. K. Khim-Farm. Zh. 1987, 21,788-801.

19. Kabanov, V. A. Polym. Sci. 1994, 36, 143-150.

20. Kabanov, V. A.; Zezin, A. B.; Rogacheva, V. B.; Gulyaeva, Zh. G.; Zansocheva,M. F.; Joosten, J. G. H.; Brackman, J. Macromolecules 1999, 32, 1904-1909.

21. Chen, W.; Turro, N. J.; Tomalia, D. A. Langmuir 2000, 16, 15.

22. Kabanov, V. A.; Sergeyev, V. G.; Pyshkina, O. A.; Zinchenko, A. A.; Zezin, A.B. Joosten, J. G. H.; Brackman, J.; Yoshikawa, K. Macromolecules 2000, 33,9587-9593.

23. Kabanov, A. V.; Kabanov, V. A. Bioconjugate. Chem. 1995, 6, 7-20.

24. B. M. Discher et al., Polymersomes: Tough Vesicles Made from Diblock Copolymers. Science 284, 1143 (05/14, 1999).

25. S. Jain, F. S. Bates, On the Origins of Morphological Complexity in Block Copolymer Surfactants. Science 300, 460 (04/18, 2003).

26. Z. Li, E. Kesselman, Y. Talmon, M. A. Hillmyer, T. P. Lodge, Multicompartment Micelles from ABC Miktoarm Stars in Water. Science 306, 98 (10/01, 2004).

27. D. J. Pochan et al., ToroidalTriblock Copolymer Assemblies. Science 306, 94 (10/01, 2004).

28. J. Raez, I. Manners, M. A. Winnik, Nanotubes from the Self-Assembly of Asymmetric Crystalline−Coil Poly(ferrocenylsilane−siloxane) Block Copolymers. Journal of the American Chemical Society 124, 10381 (09/01, 2002).

29. L. Zhang, A. Eisenberg, Multiple Morphologies of "Crew-Cut" Aggregates of Polystyrene-b-poly(acrylic acid) Block Copolymers. Science 268, 1728 (06/23, 1995).

30. R. Zheng, G. Liu, X. Yan, Polymer Nano- and Microspheres with Bumpy and Chain-Segregated Surfaces.Journal of the American Chemical Society 127, 15358 (11/01, 2005).

31. J. Cho, J. Hong, K. Char, F. Caruso, Nanoporous Block Copolymer Micelle/Micelle Multilayer Films with Dual Optical Properties. Journal of the American Chemical Society 128, 9935 (07/12, 2006).

32. J. Hong et al., Tunable superhydrophobic and optical properties of colloidal films coated with mock copolymer micelles/micelle multilayers. Adv Mater 19, 4364 (Dec 17, 2007).

33. J. Hong, K. Char, B.-S. Kim, Hollow Capsules of Reduced Graphene Oxide Nanosheets Assembled on a Sacrificial Colloidal Particle. The Journal of Physical Chemistry Letters 1, 3442 (2010).

34. H. W. Shen, L. F. Zhang, A. Eisenberg, Multiple pH-induced morphological changes in aggregates of polystyrene-block-poly(4-vinylpyridine) in DMF/H2O mixtures. Journal of the American Chemical Society 121, 2728 (05/31, 1999).

35. L. F. Zhang, A. Eisenberg, Morphogenic effect of added ions on crew-cut aggregates of polystyrene-b-poly(acrylic acid) block copolymers in solutions. Macromolecules 29, 8805 (12/30, 1996).

36. H. G. Cui, Z. Y. Chen, S. Zhong, K. L. Wooley, D. J. Pochan, Block copolymer assembly via kinetic control. Science 317, 647 (08/03, 2007).

37. G. M. Barrow, The Nature of Hydrogen Bonded Ion-Pairs - the Reaction of Pyridine and Carboxylic Acids in Chloroform. Journal of the American Chemical Society 78, 5802 (1956).

38. E. P. Parry, An Infrared Study of Pyridine Adsorbed on Acidic Solids Characterization of Surface Acidity. J Catal 2, 371 (1963).

39. Z. Gao, S. K. Varshney, S. Wong, A. Eisenberg, Block Copolymer "Crew-Cut" Micelles in Water. Macromolecules 27, 7923 (12, 1994).

40. A. Halperin, M. Tirrell, T. P. Lodge, Tethered Chains in Polymer Microstructures. Advances in Polymer Science 100, 31 (1992).

41. S. Zhong, H. G. Cui, Z. Y. Chen, K. L. Wooley, D. J. Pochan, Helix self-assembly through the coiling of cylindrical micelles. Soft Matter 4, 90 (01/07, 2008).

CHAPTER IV

Hierarchical Self-Assembly of Diblock Copolymer Blends with pH-Sensitive Coronas

4.1. Introduction

Block copolymers, which consist of chemically distinct polymer blocks, exhibit a variety of self-assembled ordered nano-phases such as spheres, cylinders, and lamellae depending on their compositions, volume fractions, and molecular weights (1). These block copolymer self-assemblies have great potential as templates for fabricating functional devices with nanoscopic periodicities (2). In particular, recent studies have demonstrated that block copolymers confined in two- and three-dimensional geometries self-assemble into ordered phase-separated domains that are observed in the bulk or anomalous microscopic phases such as helices and tori with improved directional order (3–14), which is based on pioneering works on block copolymer self-assembly in one-dimensional confined geometries (15–19). These previous studies have focused mainly on the commensurability between the characteristic length of the confining geometry and the block copolymer domain spacing. However, because methods for modifying the surfaces of such confining geometries have not been well-developed, many studies have not considered wall effects (20–22). This is especially true of confining geometries with a mobile interfacial boundary, in which the dynamics of the interface may affect the shape of the confining geometry as well as the internal phase morphology. Yang and coworkers explored the interface-driven morphological

evolution of a symmetric diblock copolymer of polystyrene-block-polybutadiene (PS-b-PB) confined in oil-in-water emulsion droplets. To control the surface preferences of the constituent PS and PB blocks at the emulsion interface, a mixture of two designed amphiphilic diblock copolymers, polystyrene-block-poly(ethylene oxide) (PS-b-PEO) and polybutadiene-block-poly(ethylene oxide) (PB-b-PEO), was used as a surfactant.

Here, we demonstrated a block copolymer mixture prepared by blending PS-b-PAA and PS-b-P4VP block copolymers at specific pH ranges without surfactant in a single phase system. Eisenberg and coworkers studied about pH-triggered inversion of vesicles from PAA-*b*-PS-*b*-P4VP and they confirmed the solution pH for preferential segregation into corona because of their relatively strong intra-corona repulsion: PAA at pH 14 and P4VP at pH 1, respectively. To extend this feature for further complexation of PS-*b*-PAA and PS-*b*-P4VP block copolymers, we suggest morphological phase separation of multi-components at extremely basic or acidic pH conditions.

In generally, morphological phase separation of block copolymers can be determined by volume fraction of each block segments, and the volume fraction can be varied by polymer solubility (mixing ratio of good and selective solvents), molecular weight ratios, and content of additives (e.g., homopolymers or counter ions). (Fig. 1) However, when two different block copolymer are mixed together, the morphology of the mixture has to be relatively compared their chemical properties.

In addition, the complexes with deformable internal morphologies were solidified by evaporating the solvent, yielding blend particles of PS-b-PAA and PS-b-P4VP with unique external shapes and internal morphologies. These colloidal particles with nanoscopic internal structures are potentially applicable to various particle-based technologies such as photonic

band gap materials (23,24), conductive particles for anisotropic conductive films based on block copolymer/metal nanoparticle composites (25,26), porous particles (27), optical actuation in microfluidic chips (28), optochemical sensing devices (29), and catalytic supports (22,30).

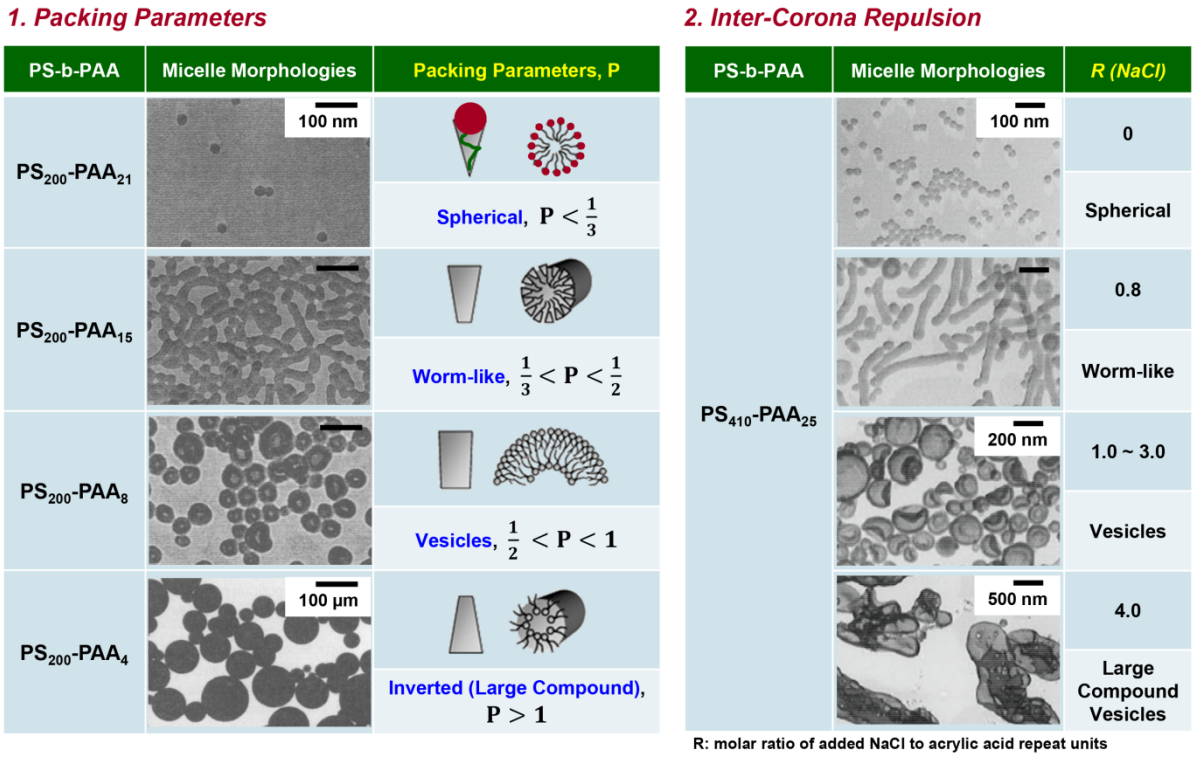

Fig 1.General parameters for self-assembly of block copolymer micelles

4.2. Experimental Section

A mixture of PS-b-PAA/PS-b-P4VP was dissolved in DMF (polymer weight: 0.49/0.81%, w/w; molar ratio: 2/3). The pH value was adjusted to 3 (or 9) using HCl (NaOH) to protonate the vinyl pyridine units (to deprotonate PAA) in order to avoid formation of complexes between PAA and P4VP. To induce micellization, water was added at a rate of 0.1% per minute to the solution until a water content of 25 %, 75 %, 99 % was reached. As controls, the micellization of PS-b-PAA and PS-b-P4VP was also preformed under the same conditions and following the same procedure.

Transmission electron microscopy was performed on a JEOL microscope with a CCD camera operating at an acceleration voltage of 80 kV. Copper TEM grids were precoated with a thin film of Formvar and then coated with carbon. A drop of solution containing 0.05 wt% of polymer was deposited on the resulting grids. Samples were dried in air overnight.

4.3. Results and Discussion

To determine the effective pH range for the inter-corona combination of PAA and P4VP dissolved together in aqueous media, we studied interaction forces between two coronas using Fourier Transfer Infrared Spectroscopy (FT-IR) as shown in Fig. 1(a) (13). It shows that dominant binding mechanism between PAA and P4VP is electrostatic interaction (1640 ~ 1650, 1500 cm-1) as well as hydrogen bonding force (1400 ~ 1450) at pH 4 (14, 15). When the solution pH decreases up to 1.0, uncharged carboxylic acid (-COOH) absorption band at about 1700 cm-1 appears. In addition, charged carboxylic acid (-COO-) absorption band seen at solution pH 14.0 has much higher peak intensity than that of peak seen at 1640 cm-1. Although mixing ratio of repeat units of two homopolymers is identical, degree of actual complexation can be controlled by solution pH. That is, when the two blocks, P4VP and PAA,

In the present study, there are two compositional parameters: solution pH to control the surface preference and DMF content to control the particle size. When we control the solution pH over 9, PAA segments can be segregated into coronas of the complexes and P4VP is not soluble in a range of pH > 5. Therefore, PS-b-P4VP block copolymers can be localized by PS-b-PAA block copolymers. As shown in Fig 2, the surface properties of the polymer particles are negative at solution pH 9. However, the complex size is not uniform by varying DMF content. In addition, even if the size of polymer particles dissolved in water 99 % and 25% is similar, the internal structure is not same. The P4VP morphology inside polymer particle dissolved in water of 99 % was spherical. However, that in water of 25 % is similar as cylindrical structures. When content of DMF is getting larger, the complex size is also

getting larger and the P4VP structures inside the particle were self-assembled into hexagonal packed cylinder structures, similar as that in bulk.

In addition, when the molecular weight of PS-b-P4VP blocks is changed for the formation of spherical structures in bulk, the complexes hierarchically self-assembled with spherical internal structures as shown in Fig. 3. In a same manner, the P4VP morphology inside polymer particle dissolved in water of 99 % was also spherical. That is, the morphology of block copolymer blends can be self-assembled into spherical structures in water-dominant environments, which is independent on molecular weights. However, the polymer particle can be aggregated into bulk morphologies in DMF-dominant environments, which is strongly dependent on molecular weights of PS-b-P4VP.

To reconfirm the pH-dependent segregation, the block copolymer blend is prepared at pH 3 as shown in Fig. 4. Although the Mw of block copolymers are varied, the morphology of polymer blend particles was observed only vesicles. That is, the morphology of block copolymer blends can be dependent on solution pH since PAA segments are also soluble under pH 4 unlike P4VP segments. Therefore, the size of the complexes is uniform even if the DMF content increases. In addition, inter-corona repulsion among P4VP segments would be very large as a result of the complex morphology of vesicles.

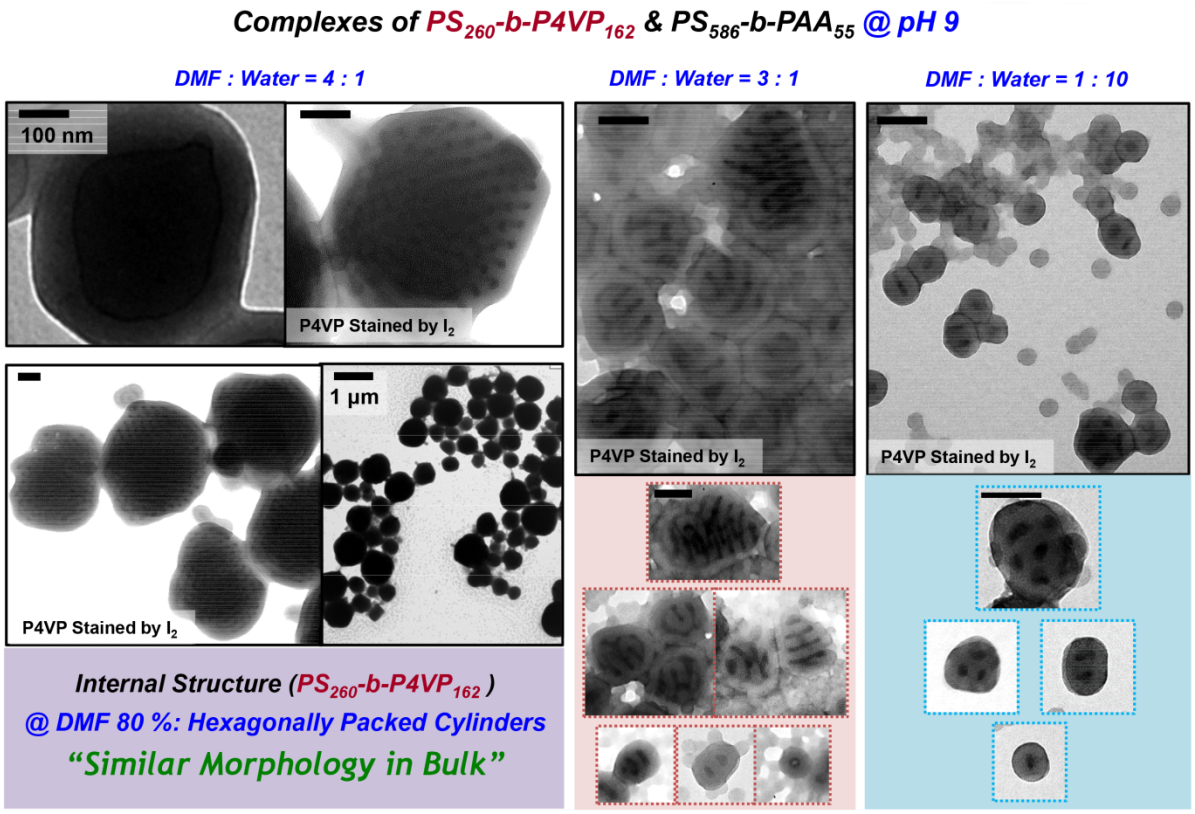

Fig. 2 Complex morphologies of PS-b-P4VP and PS-b-PAA blends prepared at pH 9 in a mixture of DMF and water

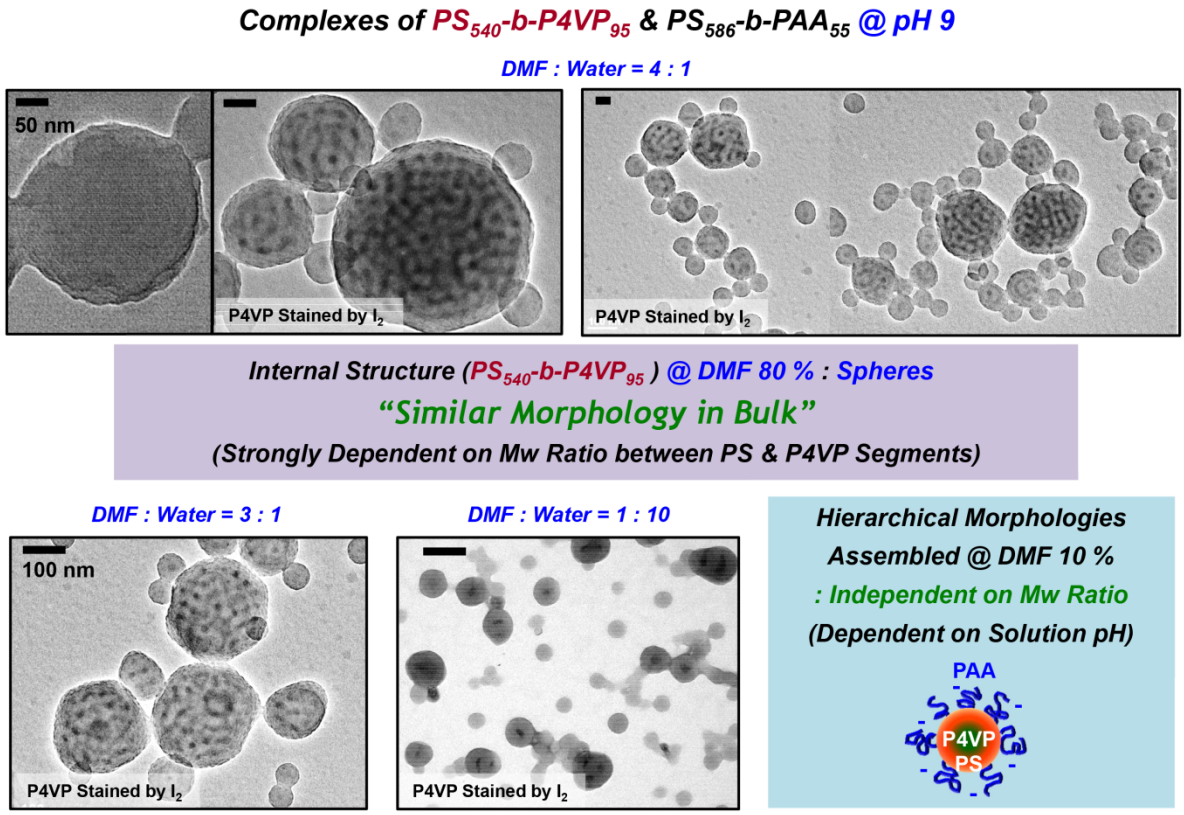

Fig. 3 Complex morphologies of PS-b-P4VP and PS-b-PAA blends prepared at pH 9 in a mixture of DMF and water

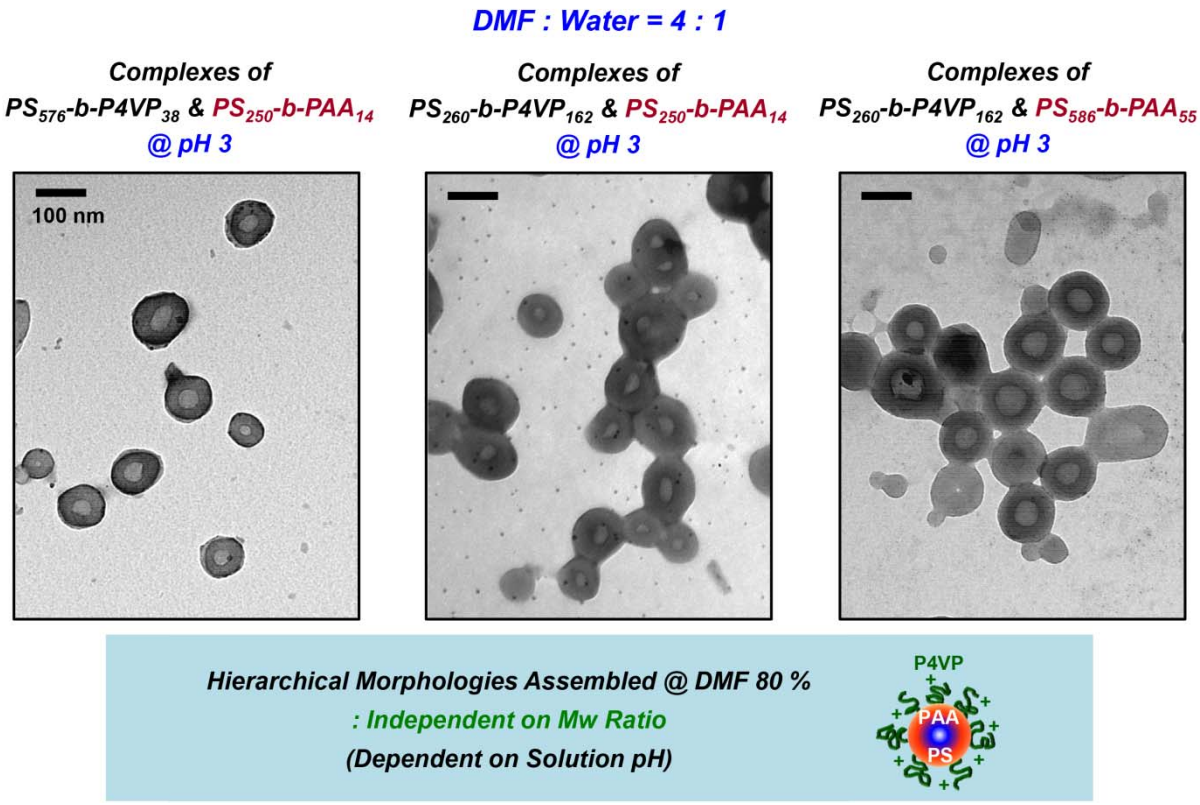

Fig. 4 Complex morphologies of PS-b-P4VP and PS-b-PAA blends prepared at pH 3 in a mixture of DMF and water

4.4. Conclusion

In the present study, there are two compositional parameters: solution pH to control the surface preference and DMF content to control the particle size. When we control the solution pH over 9, PAA segments can be segregated into coronas of the complexes and P4VP is not soluble in a range of pH > 5. Therefore, PS-b-P4VP block copolymers can be localized by PS-b-PAA block copolymers. The surface properties of the polymer particles are negative at solution pH 9. However, the complex size is not uniform by varying DMF content. In addition, even if the size of polymer particles dissolved in water 99 % and 25% is similar, the internal structure is not same. The P4VP morphology inside polymer particle dissolved in water of 99 % was spherical. However, that in water of 25 % is similar as cylindrical structures. When content of DMF is getting larger, the complex size is also getting larger and the P4VP structures inside the particle were self-assembled into hexagonal packed cylinder structures, similar as that in bulk.

In addition, when the molecular weight of PS-b-P4VP blocks is changed for the formation of spherical structures in bulk, the complexes hierarchically self-assembled with spherical internal structures. In a same manner, the P4VP morphology inside polymer particle dissolved in water of 99 % was also spherical. That is, the morphology of block copolymer blends can be self-assembled into spherical structures in water-dominant environments, which is independent on molecular weights. However, the polymer particle can be aggregated into bulk morphologies in DMF-dominant environments, which is strongly dependent on molecular weights of PS-b-P4VP.

4.5. References

1. G. H. Fredrickson, F. S. Bates, Annu. Rev. Mater. Sci. 1996, 26, 501.

2. F. S. Bates, Science 1991, 251, 898.

3. S. O. Kim, H. H. Solak, M. P. Stoykovich, N. J. Ferrier, J. J. de Pablo, P.F. Nealey, Nature 2003, 424, 411.

4. M. P. Stoykovich,M.Muller, S. O. Kim, H. H. Solak, E. W. Edwards, J.J. de Pablo, P. F. Nealey, Science 2005, 308, 1442.

5. Y. Wu, G. Cheng, K. Katsov, C. W. Sides, J. Wang, J. Tang, G. H.Fredrickson, M. Moskovits, G. D. Stucky, Nat. Mater. 2004, 3, 816.

6. K. Shin, H. Xiang, S. I. Moon, T. Kim, T. J. McCarthy, T. P. Russell,Science 2004, 306, 76.

7. B. Yu, P. Sun, T. Chen, Q. Jin, D. Ding, B. Li, A.-C. Shi, Phys. Rev.Lett. 2006, 96, 138306.

8. B. Yu, B. Li, Q. Jin, D. Ding, A.-C. Shi, Macromolecules 2007, 40,9133.

9. J. Chai, D. Wang, X. Fan, J. M. Buriak, Nat. Nanotechnol. 2007, 2,500.

10. G. E. Stein, E. J. Kramer, X. Li, J. Wang, Phys. Rev. Lett. 2007, 98,086101.

11. A. C. Arsenault, D. A. Rider, N. Tetreault, J. I. L. Chen, N. Coombs,G. A. Ozin, I. Manners, J. Am. Chem. Soc. 2005, 127, 9954.

12. a) H. Yabu, T. Higuchi, M. Shimomura, Adv. Mater. 2005, 17, 1062.b) T. Higuchi, A.

Tajima, H. Yabu, M. Shimomura, Soft Matter 2008, 4,302.

13. E. L. Thomas, J. R. Reffner, J. Bellare, J. Phys. Colloques 1990, 51,363.

14. D. M. Anderson, J. Bellare, J. T. Hoffman, D. Hoffman, J. Gunther,E. L. Thomas, J. Colloid Interface Sci. 1992, 148, 398.

15. P. Lambooy, T. P. Russell, G. J. Kellogg, A. M. Mayes, P. D.Gallagher, S. K. Satija, Phys. Rev. Lett. 1994, 72, 2899.

16. J. Y. Lee, Z. Shou, A. C. Balazs, Phys. Rev. Lett. 2003, 91, 136103-1.

17. Q. Wang,Q.Yan, P. F.Nealey, J. J. de Pablo, J. Chem. Phys. 2000, 112,450.

18. G. Krausch, R. Magerle, Adv. Mater. 2002, 14, 1579.

19. G. J. Kellogg, D. G. Walton, A. M. Mayes, P. Lambooy, T. P. Russell,P. D. Gallagher, S. K. Satija, Phys. Rev. Lett. 1996, 76, 2503.

20. S.-J. Jeon, G.-R. Yi, C. M. Koo, S.-M. Yang, Macromolecules 2007, 40,8430.

21. N. Saito, R. Takekoh, R. Nakatsuru, M. Okubo, Langmuir 2007, 23,5978.

22. Z. Lu, G. Liu, H. Phillips, J. M. Hill, J. Chang, R. A. Kydd, Nano Lett.2001, 1, 683.

23. M. Bockstaller, R. Kolb, E. L. Thomas, Adv. Mater. 2001, 13, 1783.

24. G.-R. Yi, V. N. Manoharan, S. M. Klein, K. R. Brzezinska, D. J. Pine,F. F. Lange, S.-M. Yang, Adv. Mater. 2002, 14, 1137.

25. B. B. Thompson, V. V. Ginzburg, M. W. Matsen, A. C. Balazs, Science2001, 292, 2469.

26. J. J. Chiu, B. J. Kim, E. J. Kramer, D. J. Pine, J. Am. Chem. Soc. 2005,27, 5036.

27. S.-M. Yang, N. Coombs, G. A. Ozin, Adv. Mater. 2000, 12, 1940.

28. A. Fernandez-Nieves, G. Cristobal, V. Garces-Chavez, G. C. Spalding,K. Dholakia, D. A. Weitz, Adv. Mater. 2005, 17, 680.

29. A. Setaro, S. Lettieri, P. Maddalena, L. De Stefano, Appl. Phys. Lett.2007, 91, 051921.

30. T. Ishida, M. Haruta, Angew. Chem, Int. Ed. 2007, 46, 7154.

31. G. H. Fredrickson, K. Binder, J. Chem. Phys. 1989, 91, 7265.

32. P. C. Hohenberg, J. B. Swift, Phys. Rev. E 1995, 52, 1828.

33. R. A. Wickham, A.-C. Shi, Z.-G. Wang, J. Chem. Phys. 2003, 118,10293.

34. S. Koizumi, H. Hasegawa, T. Hashimoto, Macromolecules 1994, 27,6532.

35. G. J. A. Sevink, A. V. Zvelindovsky, Macromolecules 2005, 38,7502.

36. T. Q. Chastek, T. P. Lodge, J. Polym. Sci, Part. B: Polym. Phys. 2006,44, 481.

37. H. Morita, T. Kawakatsu, M. Doi, D. Yamaguchi, M. Takenaka,T. Hashimoto, Macromolecules 2002, 35, 7473.

국문초록

본 연구에서는 고분자 전해질을 이용하여 구현할 수 있는 대표적인 두 시스템인, 고분자 복합체 (polyelectrolyte complex)와 고분자 다층박막(polyelectrolyte multilayer thin film)에 대하여 다루었다. 고분자 복합체는 반대의 전하를 갖는 두 고분자 전해질을 수용액 상에서 자유롭게 반응시켜 구현할 수 있고, 이러한 고분자 복합체 시스템 중에서 특히, 두 고분자 전해질을 순차적으로 기판 위에 정렬시켜 박막의 형태로 구현한 것을 고분자 다층박막이라고 할 수 있는데, 본 연구에서는 아래의 네 가지 부분으로 나누어 정리하였다.

첫째, 다층박막을 구현하는 기존의 방법과는 다른, 미세유체소자를 이용한 창의적인 방법을 제안하였다. 즉, 반대의 전하를 갖는 두 고분자 전해질 용액을 액적(alternating droplets)의 형태로 만들어 교대로 발생시킴으로써, 다층박막을 쌓고자 하는 기판인 마이크로 입자와 충돌시켜 다층박막을 구현할 수 있었다. 기존의 방법으로는 마이크로 입자 위에 쌓을 수 있는 두께에 한계가 있었고, (< 10 bilayers) 사용되는 시약의 양이나 박막을 구현하는데 필요한 시간의 제약이 있었던 것이 사실이었다. 즉, 본 연구는 훨씬 적은 양의 시약으로 빠른 시간 내에 쉽게, 기존의 방법으로는 할 수 없었던 마이크로 단위의 두꺼운 다층박막을 마이크로 입자 위에 구현해 낼 수 있었다.

둘째, 앞서 제시한 미세유체소자를 이용하여 쌓은 다층박막을 층류(laminar flow)를 이용하여 선택적으로 해리시켜 야누스(janus) 모양의 다층박막을 구현하는 연구를 수행하였다. 다층박막 간에 존재하는 결합을 분해시킬 수 있는 용매를 미세유체 소자 내의 층류의 형태로 다층박막과 접촉시킴으로써 지속적인 해리반응을

유도하여, 기존의 방법으로는 구현할 수 없는 독창적인 방법을 구현하였고, 이를 통해 야누스 모양의 다층박막을 제안할 수 있었다. 이러한 연구는 우리 몸의 모세혈관의 환경을 모사할 수 있는데, 즉, 전단응력이 존재하고 마이크로 크기의 너비를 갖는 실험 환경을 제시함으로써, 본 연구는 생체 내의 실험을 구현할 수 있는 모델 시스템으로써 제안할 수 있다.

셋째, 반대의 전하를 갖는 두 블록공중합체 미셀(block copolymer micelle)을 이용하여 수용액상에서 코로나 간의 정전기적 상호작용을 이용하여 미셀 복합체를 구현하는 연구를 제안하였다. 이러한 블록공중합체 미셀은 코로나를 구성하는 고분자 간의 반발력이 감소되면 미셀 구조가 쉽게 변화된다고 알려져 있다. 따라서 본 연구에서는 용액의 pH에 따라 이온화도가 쉽게 조절되는 고분자를 코로나로 사용하여 실험을 진행하였다. 즉, 반대의 전하를 갖는 코로나 간의 복합체를 유도하여 구형의 미셀 코로나를 중성화시킴으로써, 미셀 자체의 구조의 변화를 유도하여 기존에 보고된 바 없는 복합체 구조를 구현하였다. 또한 코로나 간의 반발력은 용액의 pH에 따라 조절하여 고분자 미셀 복합체의 구조를 미세하게 변화시킬 수 있었다.

넷째, 용액의 pH에 따라 경쟁적으로 이온화되려는 경향성을 갖는 두 고분자를 각 블록의 코로나로 지정하여 계층적인 구조를 갖는 미셀 복합체를 구현하였다. 즉, 두 고분자가 함께 녹아있는 경우, 특정 pH에서 두 고분자 중 하나가 우선적으로 코로나가 되려는 경향성이 있어, 이러한 특성을 바탕으로 복합체에서의 각 블록의 위치를 pH에 의해서 쉽게 조절할 수 있었다. 또한 코어부분에 위치한 블록공중합체의 경우에는 용매의 조건에 따라 벌크에서와 같이 분자량 비율에 따른 미세 상분리 구조를 유도할 수 있었다.

즉, 미세유체소자를 이용하여 다층박막을 구현할 수 있는 방법을 제안하였고, 구조가 쉽게 변할 수 있는 블록공중합체 미셀의 표면특성을 조절함으로써 독특한 미셀 복합체 구조를 제안할 수 있었다. 이처럼 본 연구는 누구도 진행한 바 없는 창의적인 연구로서, 전 세계의 관련 연구와 비교했을 때 그 차별성과 독창성이 인정된다.

주요어: 다층박막, 복합체, 고분자전해질, 블록공중합체 미셀, 정전기적 인력

학번: 2009-30246